Biophysical Interactions of Plankton with Environments: From Individual Locomotion to Population Dynamics

Bacteria Locomotion near a no-slip Wall

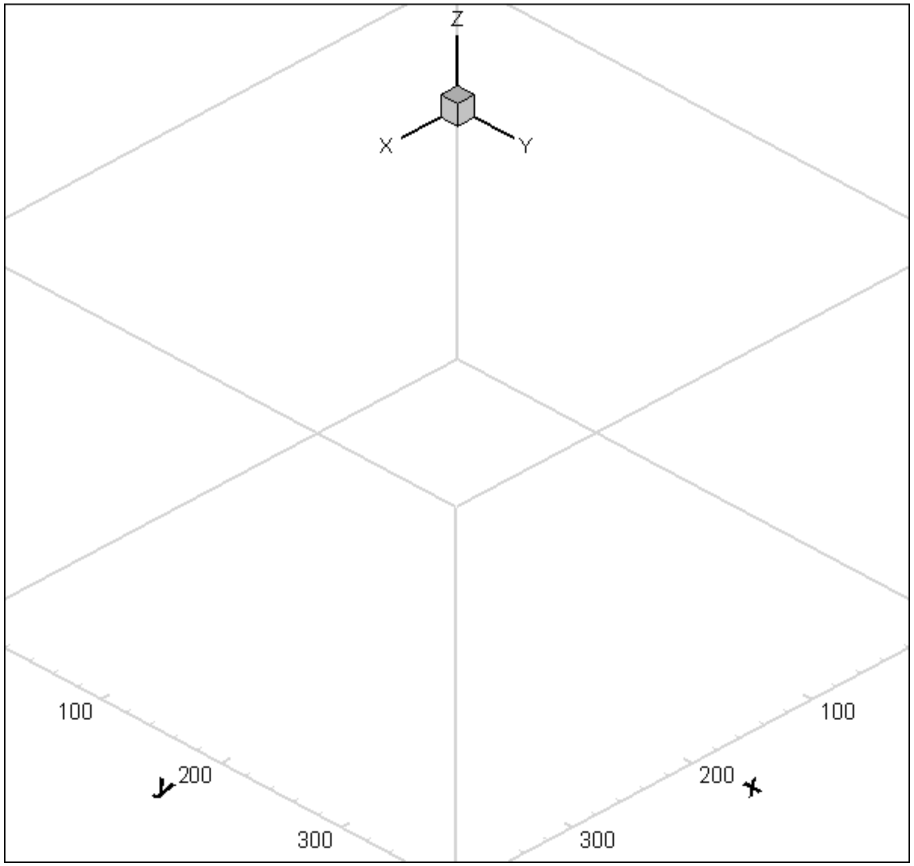

***Oxyrrhis* in Motion**

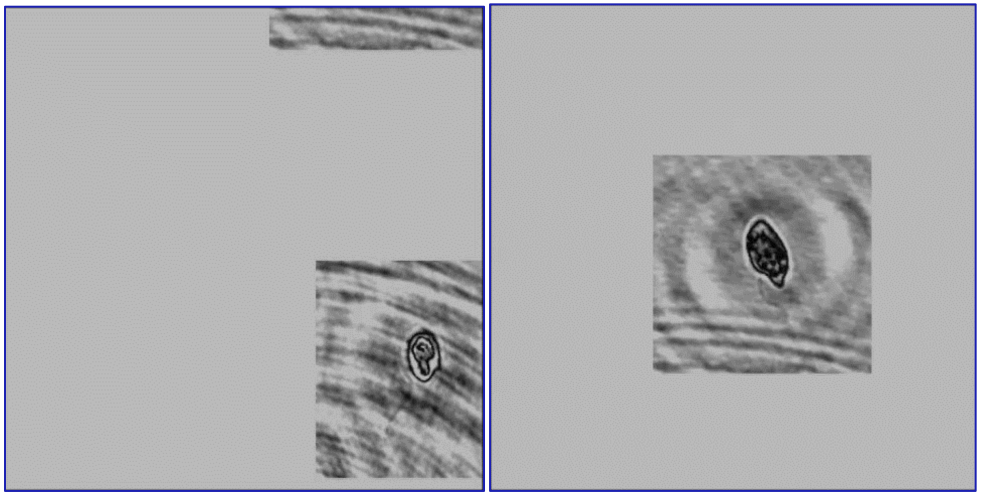

Bacteria and Droplets Interactions

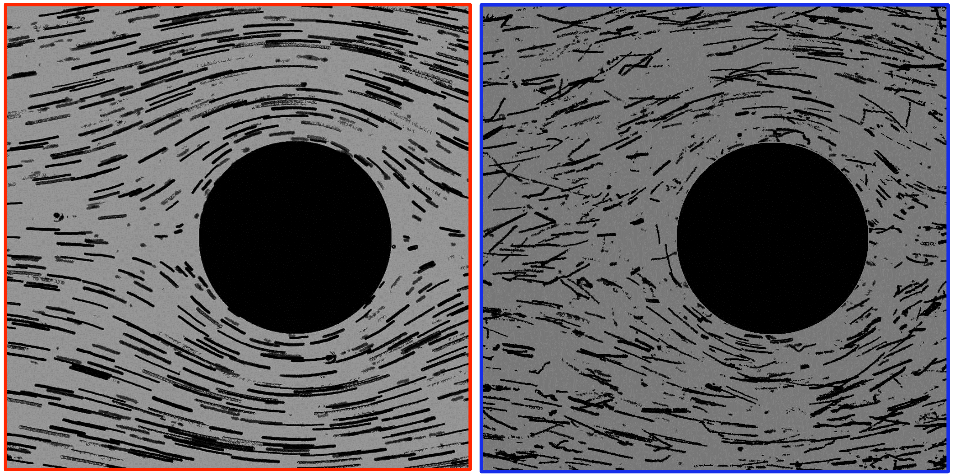

Jian Sheng

SIAM Conference on Mathematics of Planet Earth

Philadelphia, Pennsylvania USA

Texas A&M University

Molaei & Sheng, *et al.*, Phys. Rev. Lett, 2014

Molaei & Sheng *et al.*, (sumbitted)

Objective: Mechanistic Understanding of Plankton-Environment Interaction

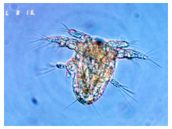

Compensatory escape mechanism at low Reynolds number - Switching to a power stroke enables a tiny marine crustacean to survive

Gemmell B., Sheng. J, PNAS 2013

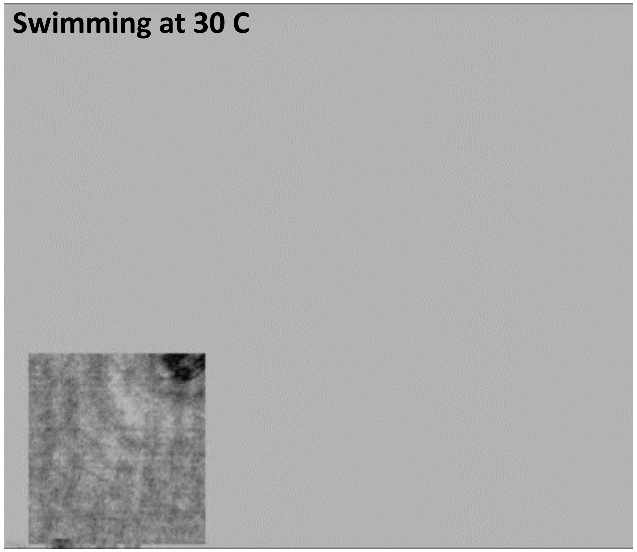

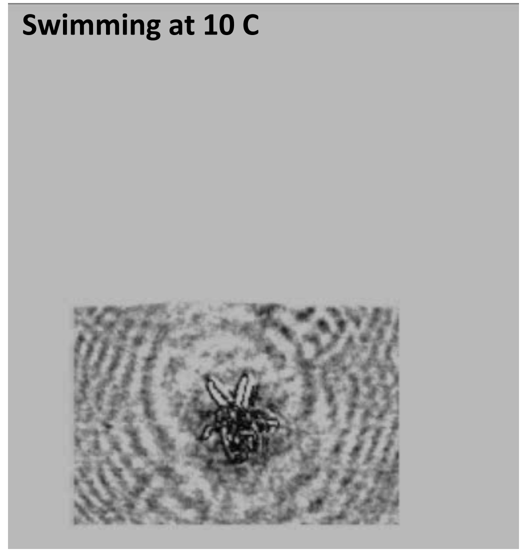

Morphology of seahorse head hydro-dynamically aids in capture of evasive prey

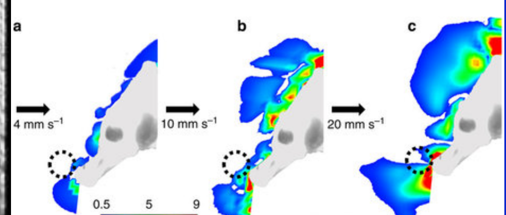

Gemmell B., Sheng. J, Nat. Comm. 2013

Biomimetic FSMA Sensor and Actuator

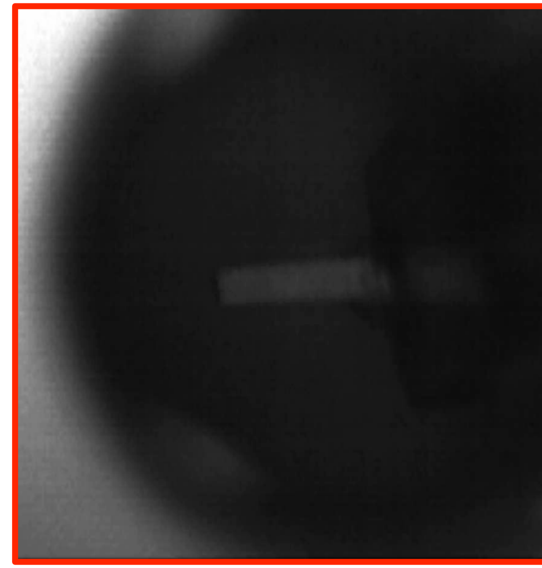

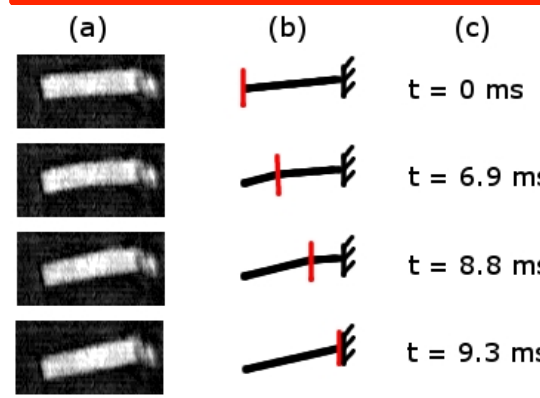

NiMnGa FSMA shear actuation mode by twin boundary propagation

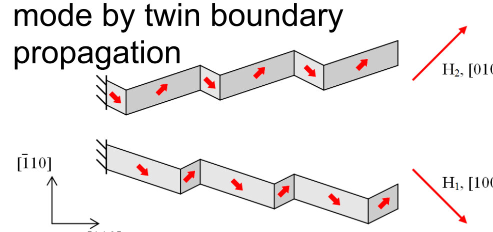

Ganor, Sheng, et al., Smart Material & Structure 2013

Methods: Engineering Complex Environment for Mechanistic Studies

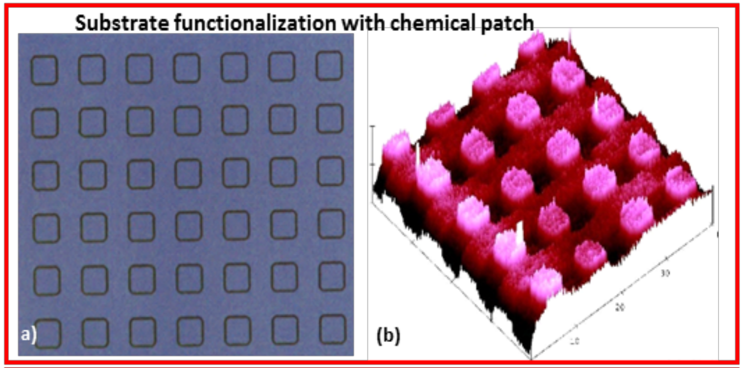

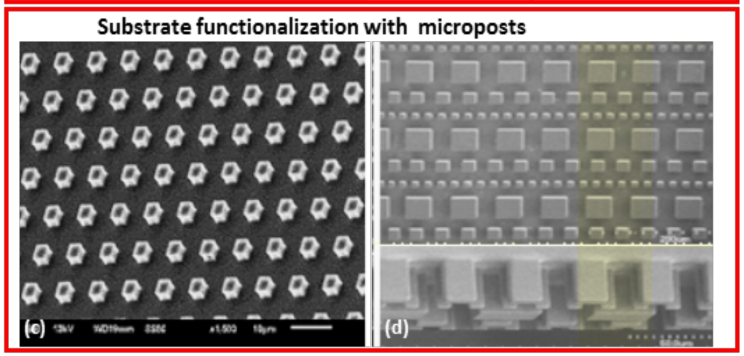

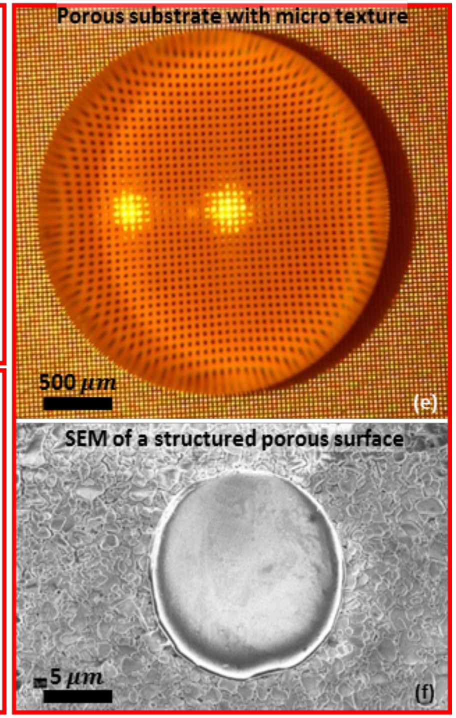

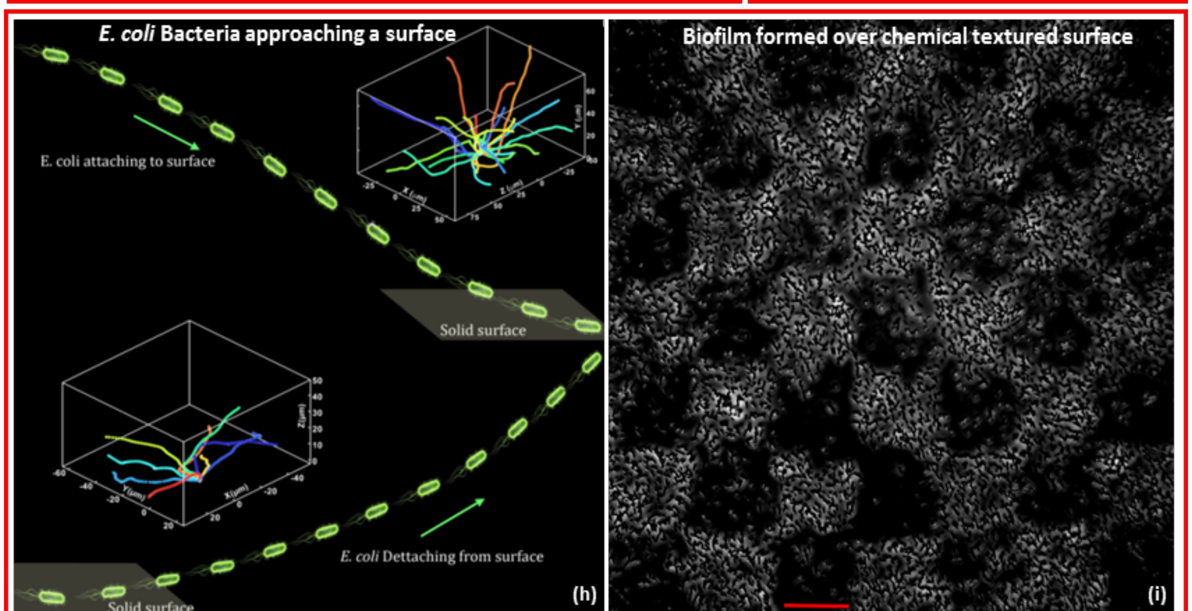

Surface characteristics

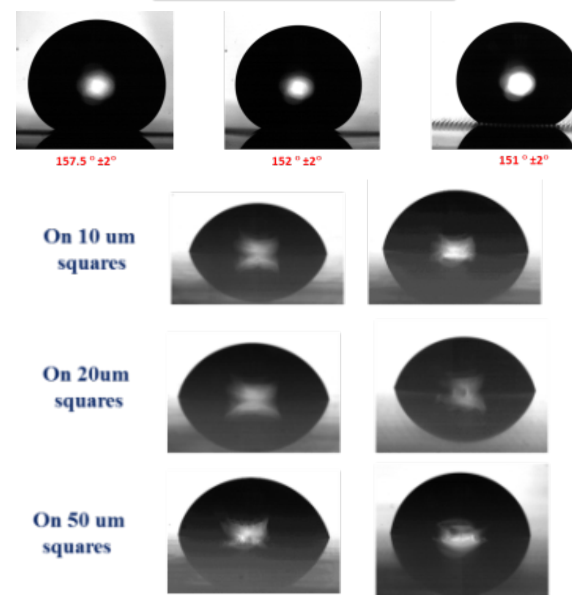

Jalali, Sheng, et al., 2014 (a,b,c) (submitted)

Methods: Digital Holography Capturing 3D Planktonic Motion

Numerical Reconstruction:

$$\tilde{U}_r(x,y,z) = \iint_{x_h, y_h} \tilde{U}_r(\xi,\eta,z=0)\left[-\tfrac{\partial G}{\partial n}(x-\xi, y-\eta, z)\right] d\xi d\eta$$

Rayleigh-Sommerfeld Near Field Diffraction

$$-\tfrac{\partial G}{\partial n}(x,y;z) = \tfrac{1}{\lambda}\frac{\exp\left(-jk\sqrt{x^2+y^2+z^2}\right)}{\sqrt{x^2+y^2+z^2}}\cos\theta$$

Kirchhoff-Fersnel Far-Field Diffraction

$$-\tfrac{\partial G}{\partial n}(x,y;z) = \frac{\exp(jkz)}{j\lambda z}\exp\left\{j\tfrac{k}{2z}\left[\left(x^2+y^2\right)\right]\right\}$$

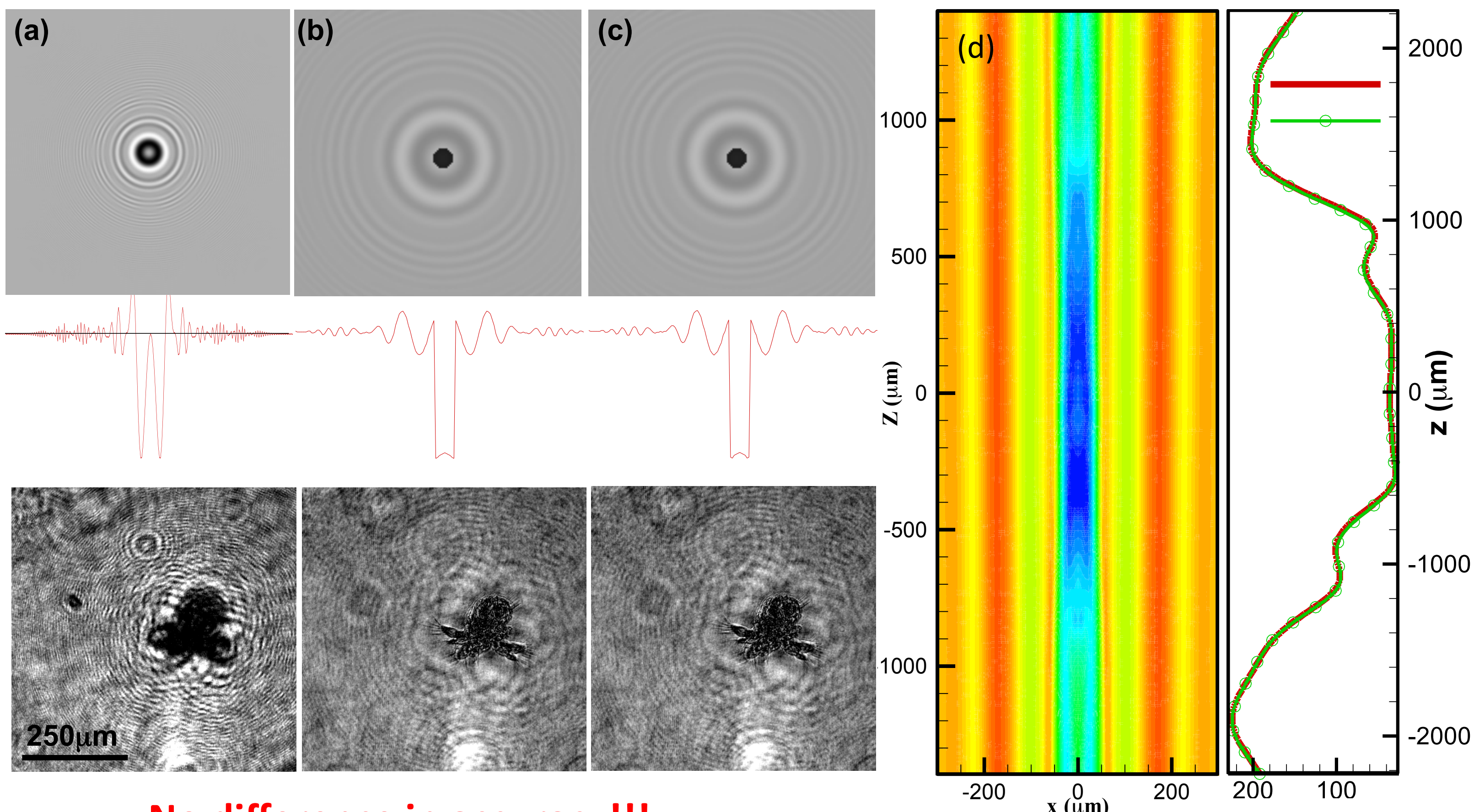

No difference in accuracy!!!

Katz & Sheng, ARFM, 2010

A Sample Reconstruction using DHM

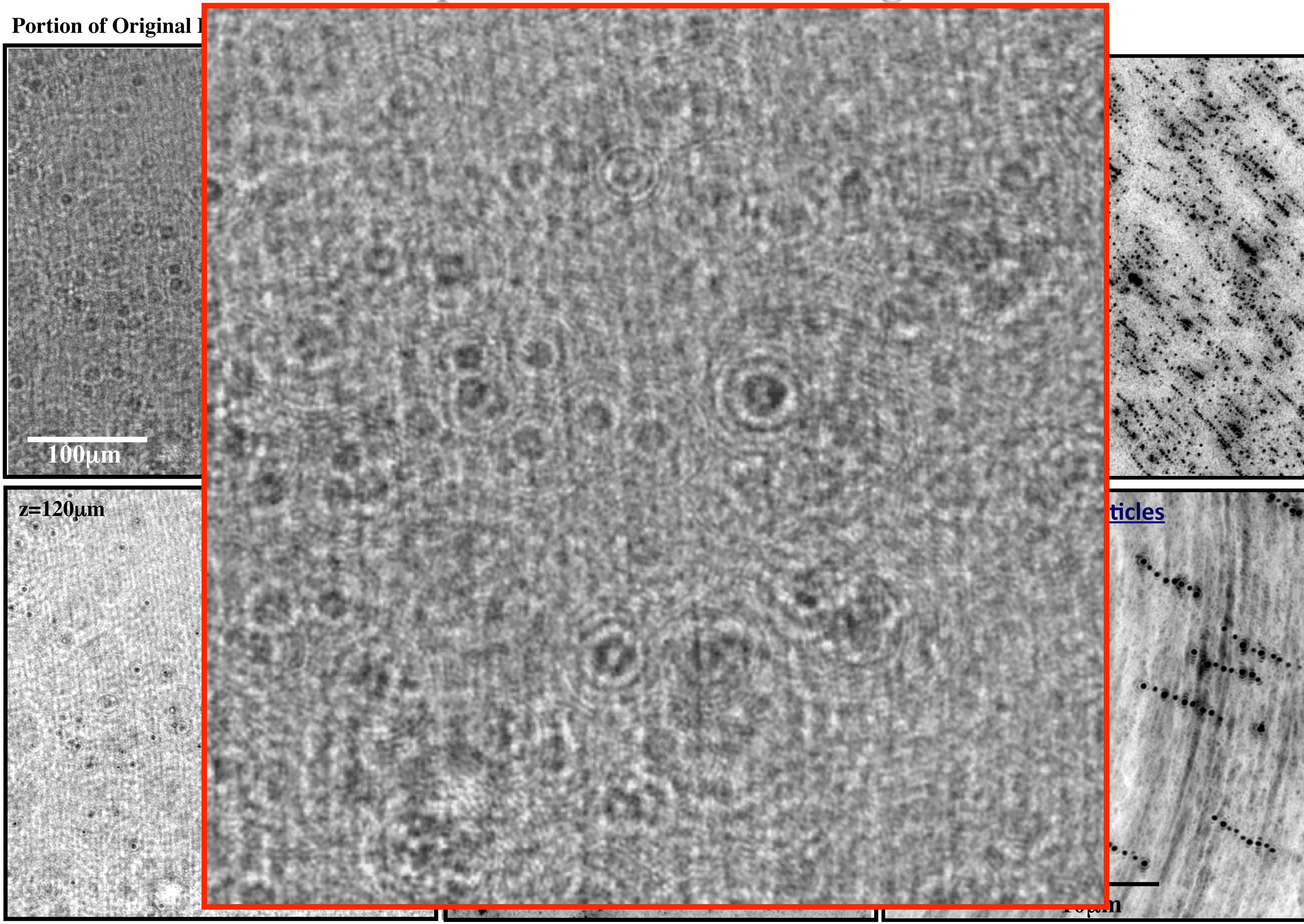

Study I: A Mixotrophic Dinoflagellate Stuns Prey Prior to Ingestion – Key Predator Prey Mechanism for Harmful Algal Bloom

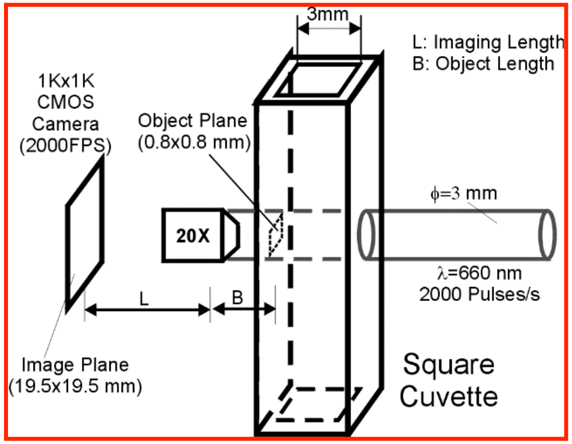

Supported by: NSF, ONR

Karlotoxins

Geographic distribution of karlotoxins

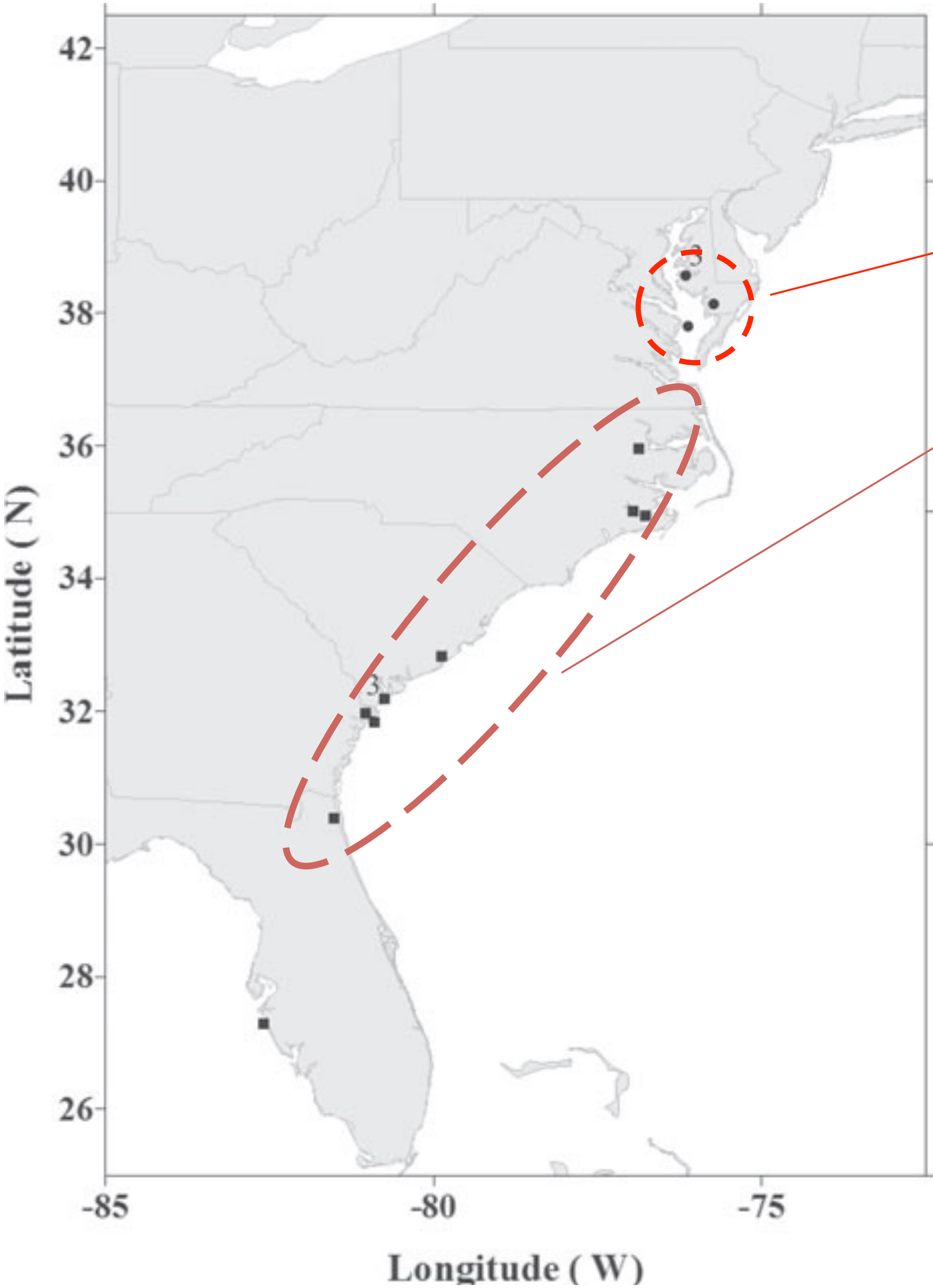

Structures of karlotoxins

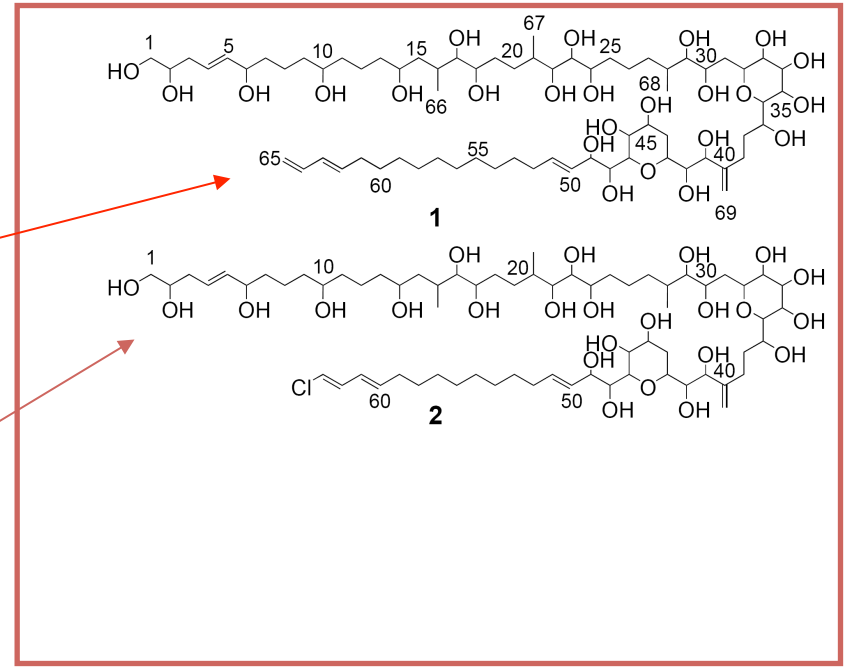

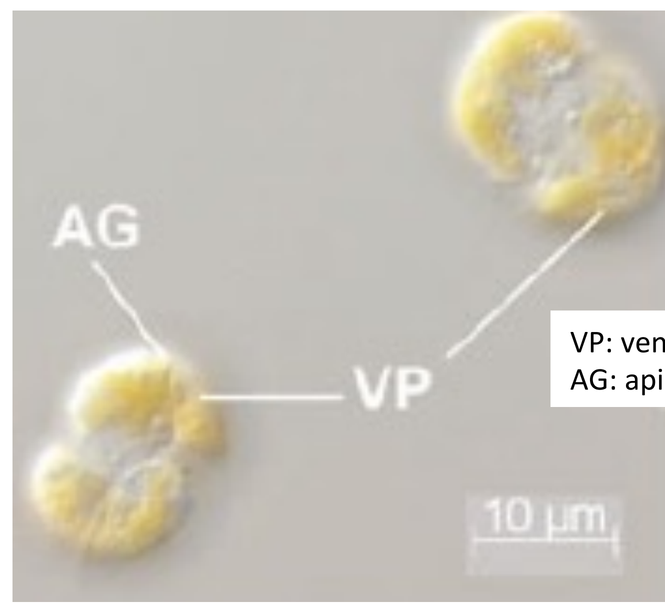

VP: ventral pore
AG: apical groove

Effects of Purified Karlotoxins on Prey

Swelling

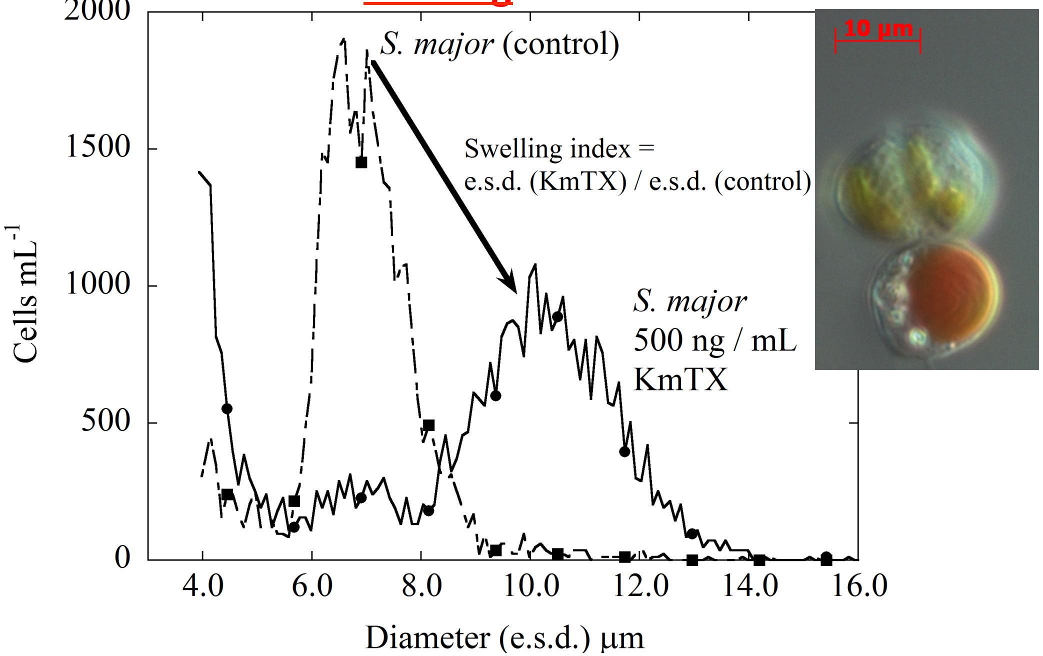

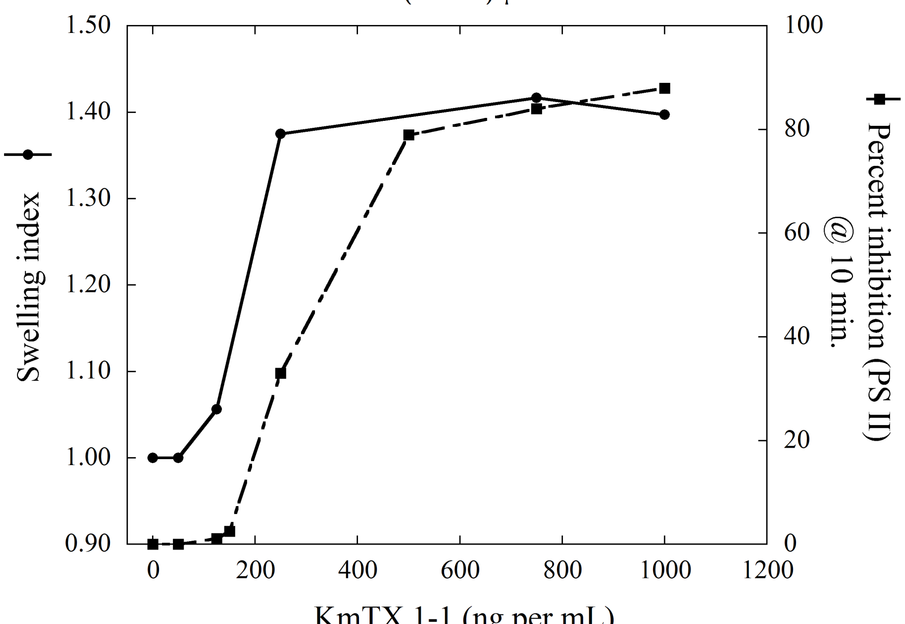

Sheng *et al.* PNAS, 2010

Toxicity Level of Karlotoxins

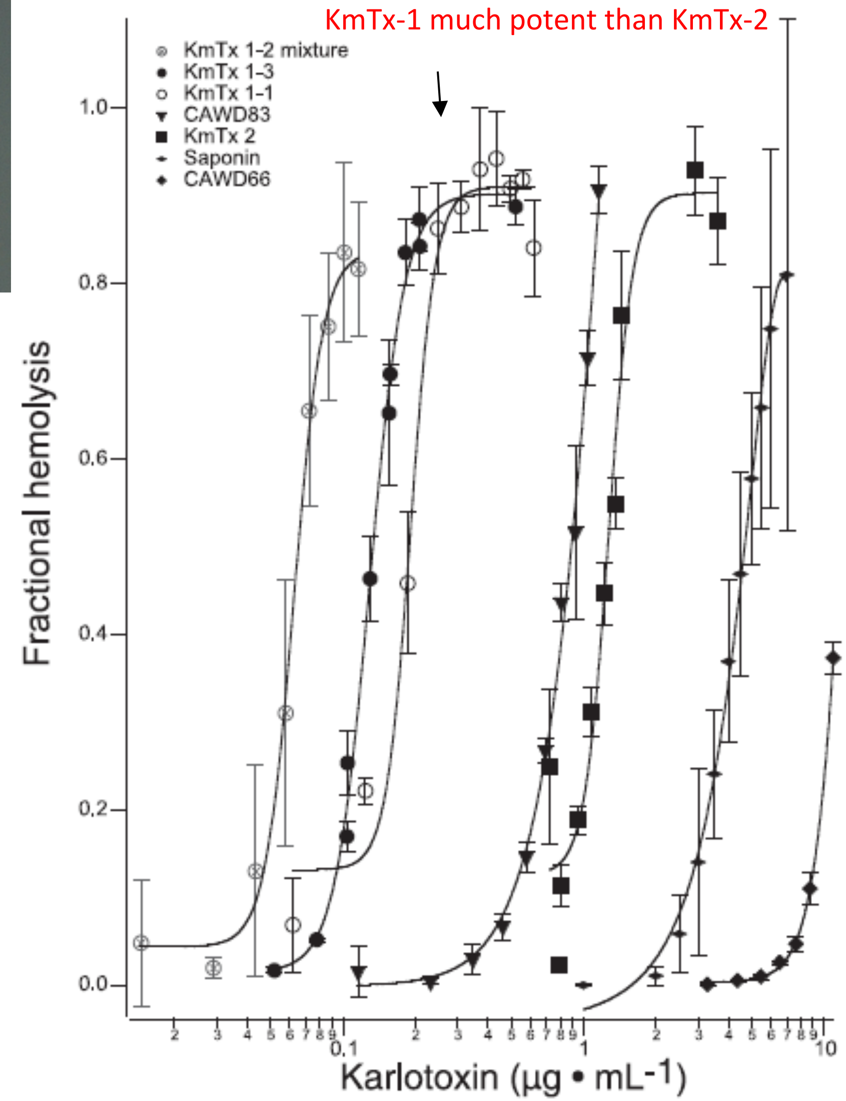

Bachvaroff *et al.*, J. of Phycology, 2009

Karlotoxin as Allelochemicals or … ? – What is Ecological Function

Inhibition of *Oxyrrhis* grazing on *toxic* strains

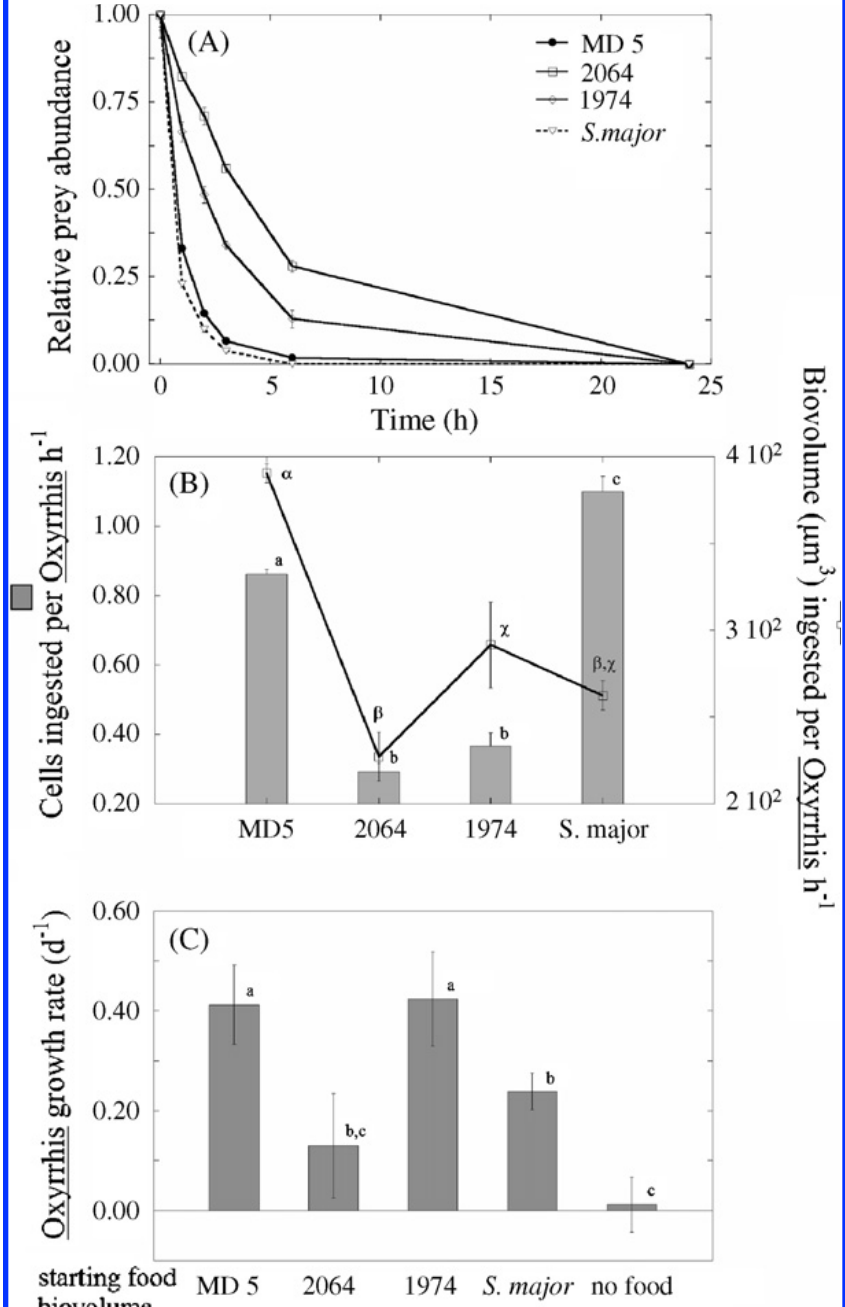

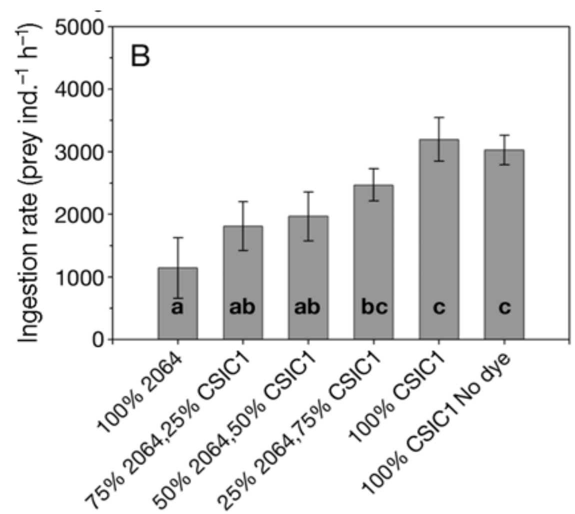

Karlotoxins mediate the grazing pressure by zooplankton species, *A. tonsa* !!!

*Waggett *et al. MEPS* 2008

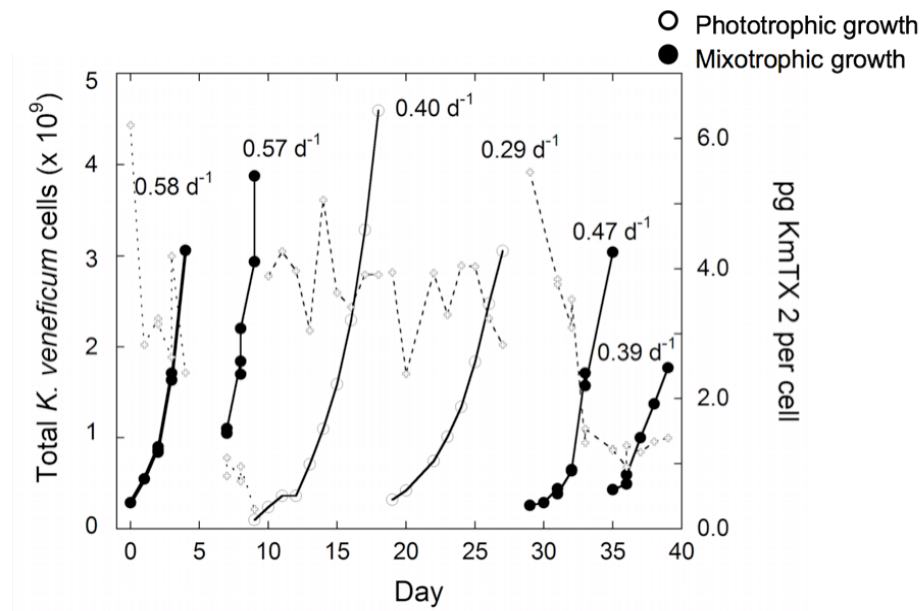

Improved mixotrophic growth over phototrophic growth by toxic strains!

Predator-Prey Interactions using 3D DHM

In-line DHM Cinematography

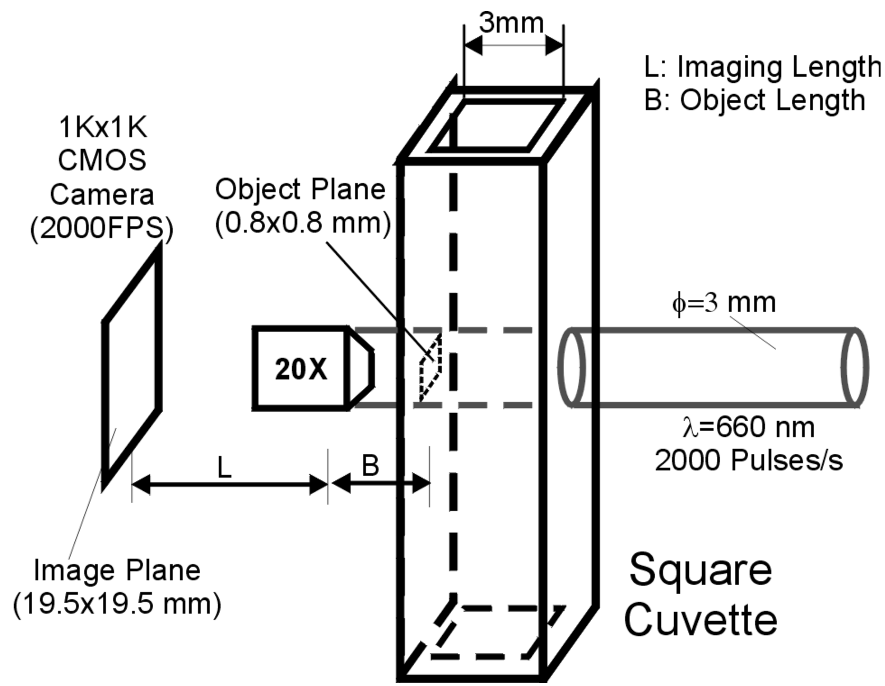

Swimming Characteristics

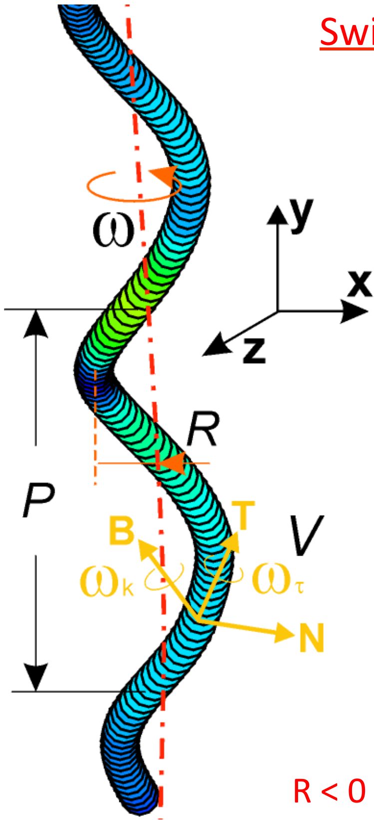

$$\vec{K}(t) = \vec{N}(t) \times \frac{d\vec{N}(t)}{dt}$$

$$V(t) = \left|\dot{\vec{r}}(t)\right|$$

$$R(t) = \frac{\left|\vec{T}(t) \times \vec{K}(t)\right|}{\sqrt{k^2 + \tau^2}}$$

$$P(t) = 2\pi \frac{\vec{T}(t) \cdot \vec{K}(t)}{\sqrt{k^2 + \tau^2}}$$

$$\vec{\omega}(t) = V(t)\sqrt{k^2 + \tau^2}\,\vec{K}(t)$$

R < 0 – Left hand helix

Swimming Induced Dispersion:

$$D_{ii} = \left\langle u_{ii}^2 \right\rangle t, i = x, y, z$$

Dispersion coefficients are determined from Lagrangian velocity autocorrelation functions

$$D_{ii}(t) = \left\langle \int_0^t d\tau \int_0^\tau R_{ii}(\eta)\, d\eta \right\rangle = \int_0^t d\tau \int_0^\tau \left\langle R_{ii}(\eta) \right\rangle$$

Taylor (1921), Snyder and Lumly (1971), Gopalan et al. (2008)

Procedures:

- Recording holograms
- Numerically reconstructing hologram plane by plane
- Tracking algorithm obtaining 3-D trajectories
- Predator and prey distinguished by in-focus images

Sheng et. al. PNAS (2007)

Experimental Conditions

Culture	Concentration (cells/ml)	Toxicity	Predation Level	prey/predator ratio	No. of cells examined	Length (µm)	Width (µm)
1974 (alone)	120,000	**KmTx-1**	High	0	981	8-10	6-8
1974 + *S. major* (h0)	350,000	High		1:1	1164		
BM1 (alone)	70,000	**KmTx-2**	Medium	0	939	6-8	4-5
BM1 + *S. major* (h0)	120,000	Medium		1:1	2328		
BM1 + *S. major* (h5)	110,000			1:1	968		
2064 (alone)	70,000	**KmTx-2**	Low	0	828	12-15	8-10
2064 + *S. major* (h0)	210,000	Low		1:1	991		
2064 + *S. major* (h5)	190,000			1:1	968		
MD5 (alone)	170,000	None	None	0	1040	8-10	6-8
MD5 + *S. major* (h0)	275,000			1:1	2234		
MD5 + *S. major* (h5)	100,000			1:1	1804		
S. Major	75,000	None			1502	6-8	
S. Major + Methanol (h5)	75,000				1611		
S. Major + KmTx-1 (h5)	75,000		2.5ng mL^{-1}		2253		
S. Major + KmTx-2 (h5)	75,000		2.8ng mL^{-1}		1301		

- Examine swimming behavior of toxic and nontoxic K. veneficum strains prior and after mixing with prey
- Examine swimming behavior of Storeatula major prior and after mixing with predator
- Measure swimming characteristics of S. major in the presence of exogenous toxins

Effects on Swimming Trajectories by Predation (Toxic Strains only)

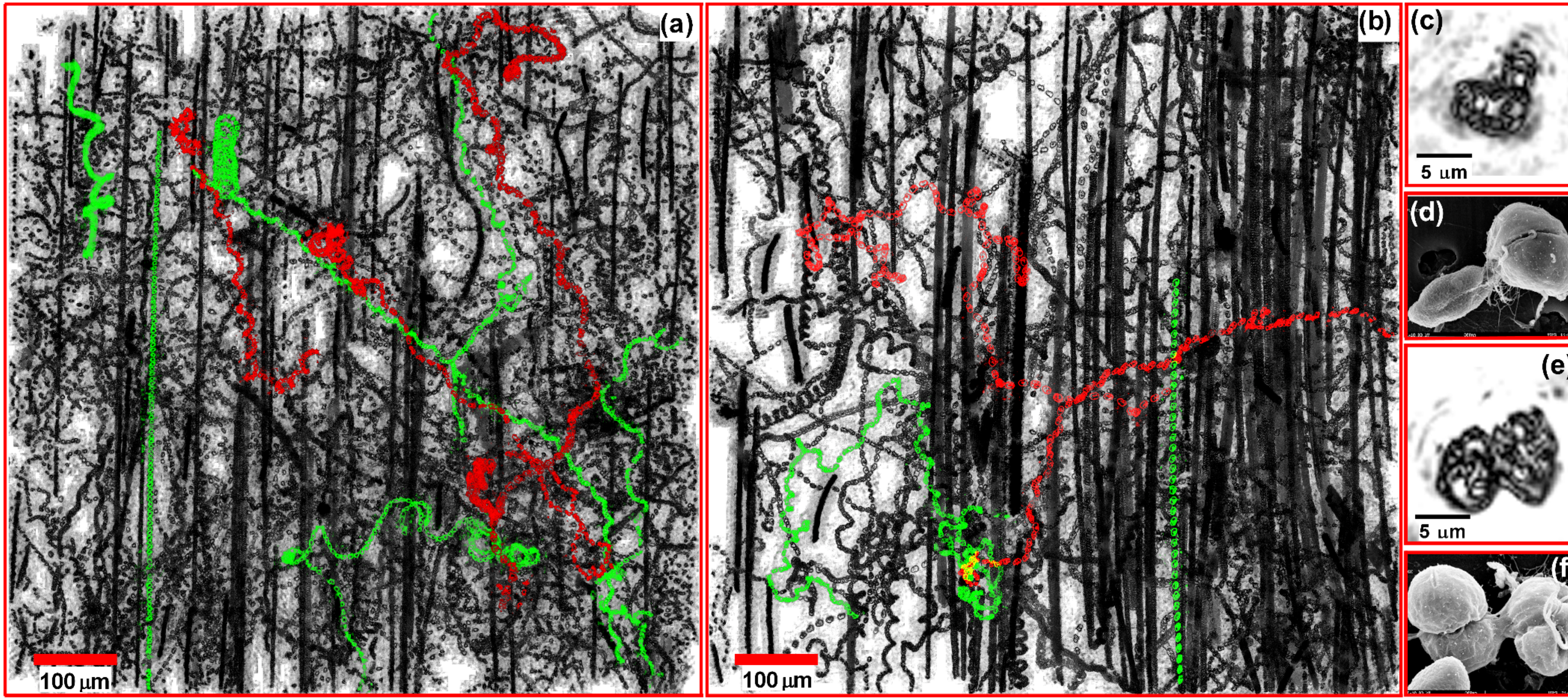

Superposition of reconstructed in-focus holographic images (only one of every five exposures is shown for clarity): Gray trajectories - tracks of prey, *S. major.* (only), after introduction to a *K. veneficum*, BM1 suspension; Green - highlighted samples of *S. major* trajectories; Red - few sample *K. veneficum* BM1 (predator) trajectories (rest of the BM1 tracks are not shown). (a) Shortly after mixing; (b) 5 hours later; (c and d) Captured *S. major* cells (smaller ones) being ingested by a BM1 cell: (c) a reconstructed hologram, and (d) SEM. (e and f) Pair of *K. veneficum*, BM1 cells interacting (possibly cell division) : (e) reconstructed hologram, (f) SEM. Vertical linear tracks belong to immotile prey; convection by the background flow causes their linear motion, which is subtracted while calculating velocity. Scales: 100 mm in a & b, and 5 mm in c & e. The complex motions of motile cells, and increasing fraction of immotile ones with time are evident

Substantial Difference in Swimming Characteristics among Strains

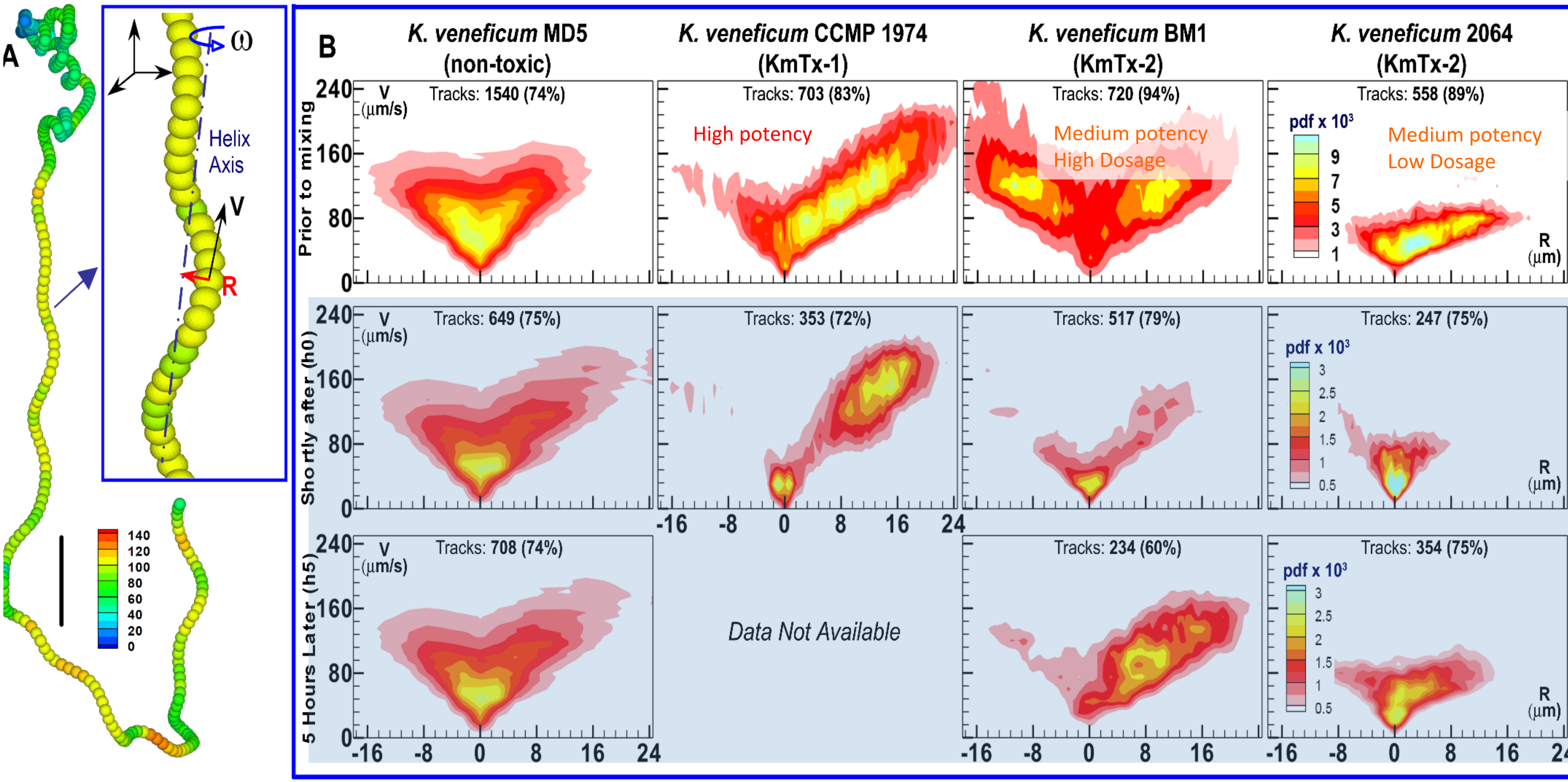

- Substantial variations in swimming characteristics among strains

Modes of bi-flagellated Motion

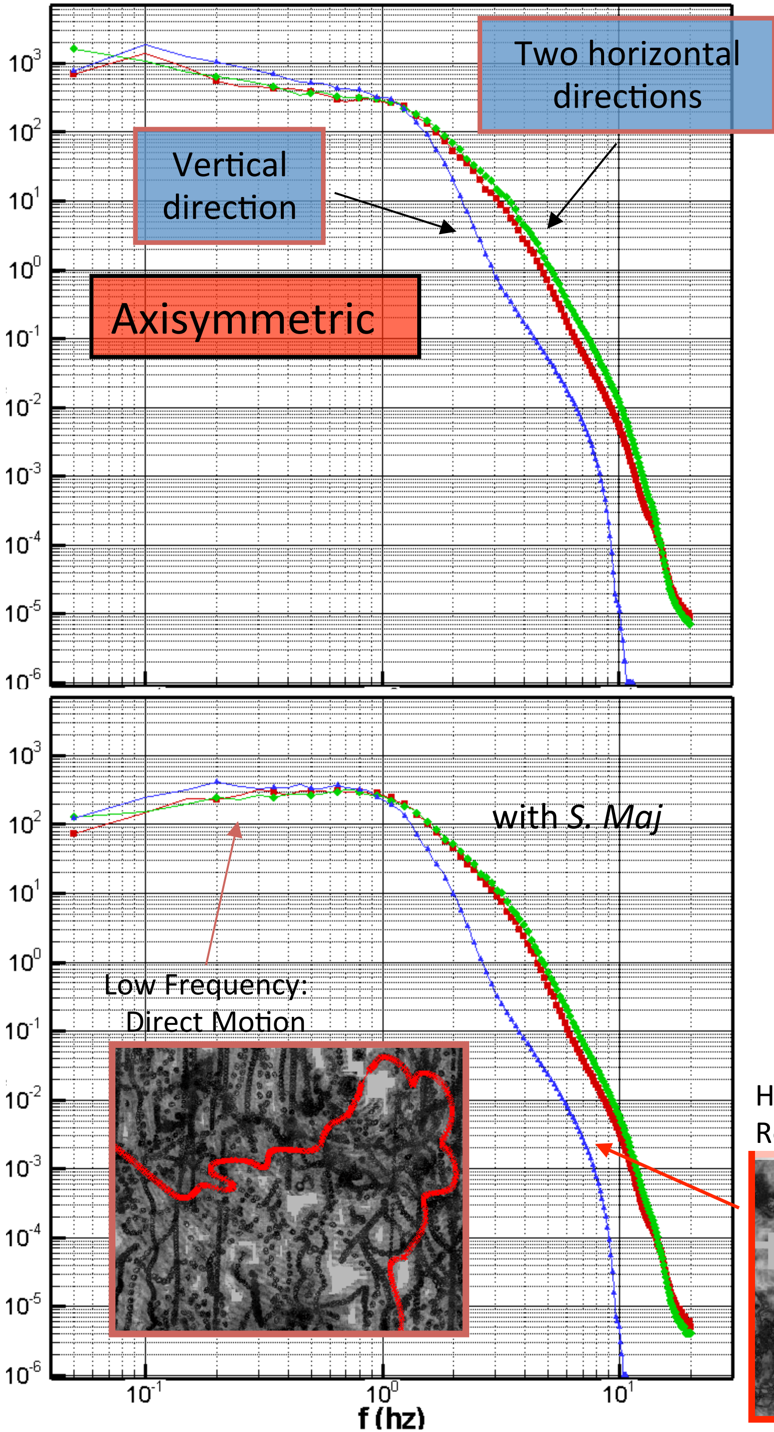

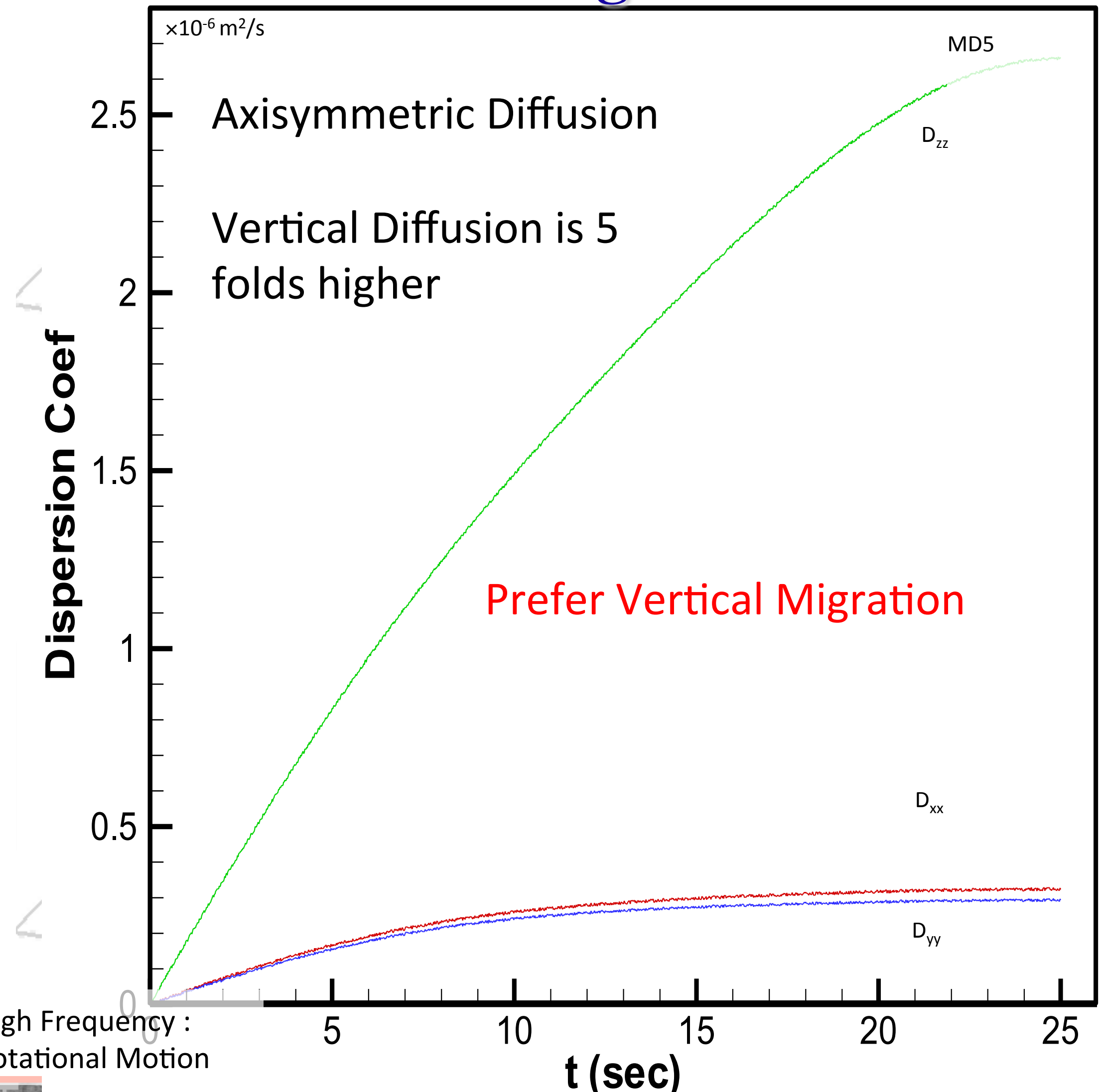

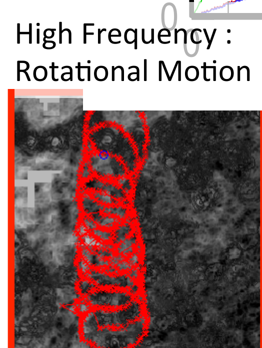

- *K. veneficum* prefer vertical motion
- Axisymmetric bi-flagellated motions

Variability in 3-D Trajectories

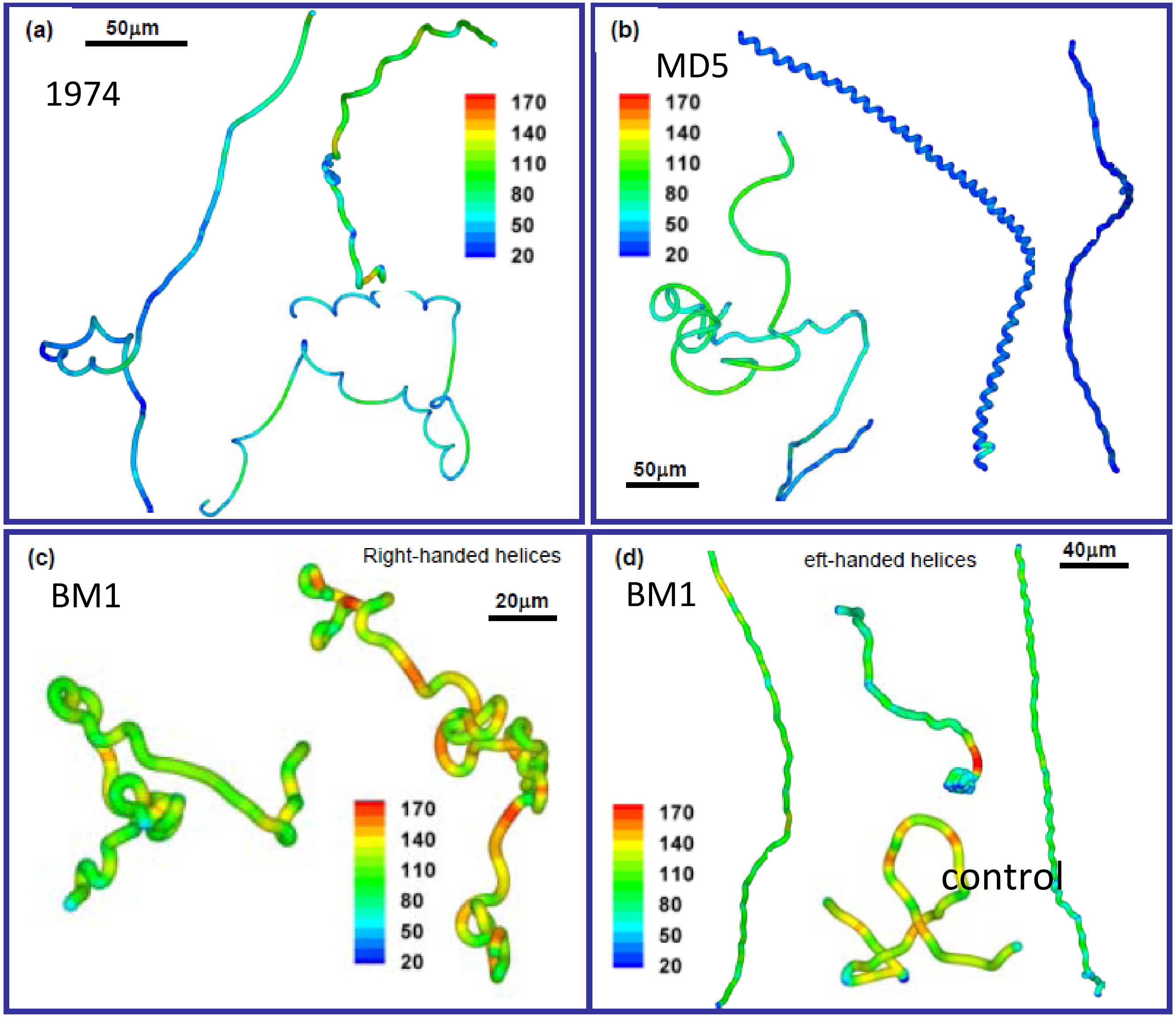

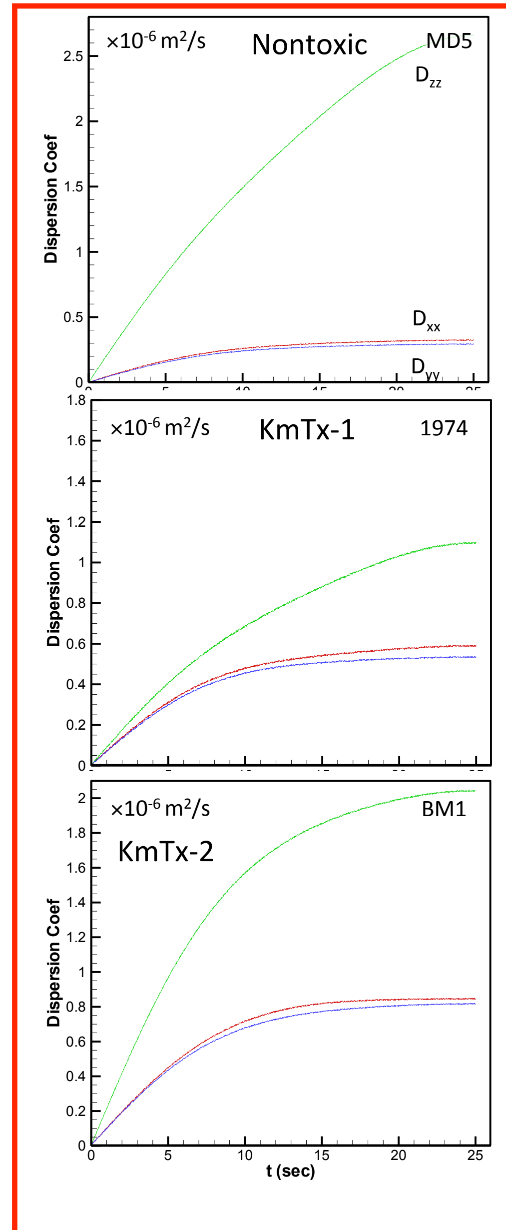

Colored coded by velocity magnitude.

Predation Mediated Changes in Swimming Characteristics

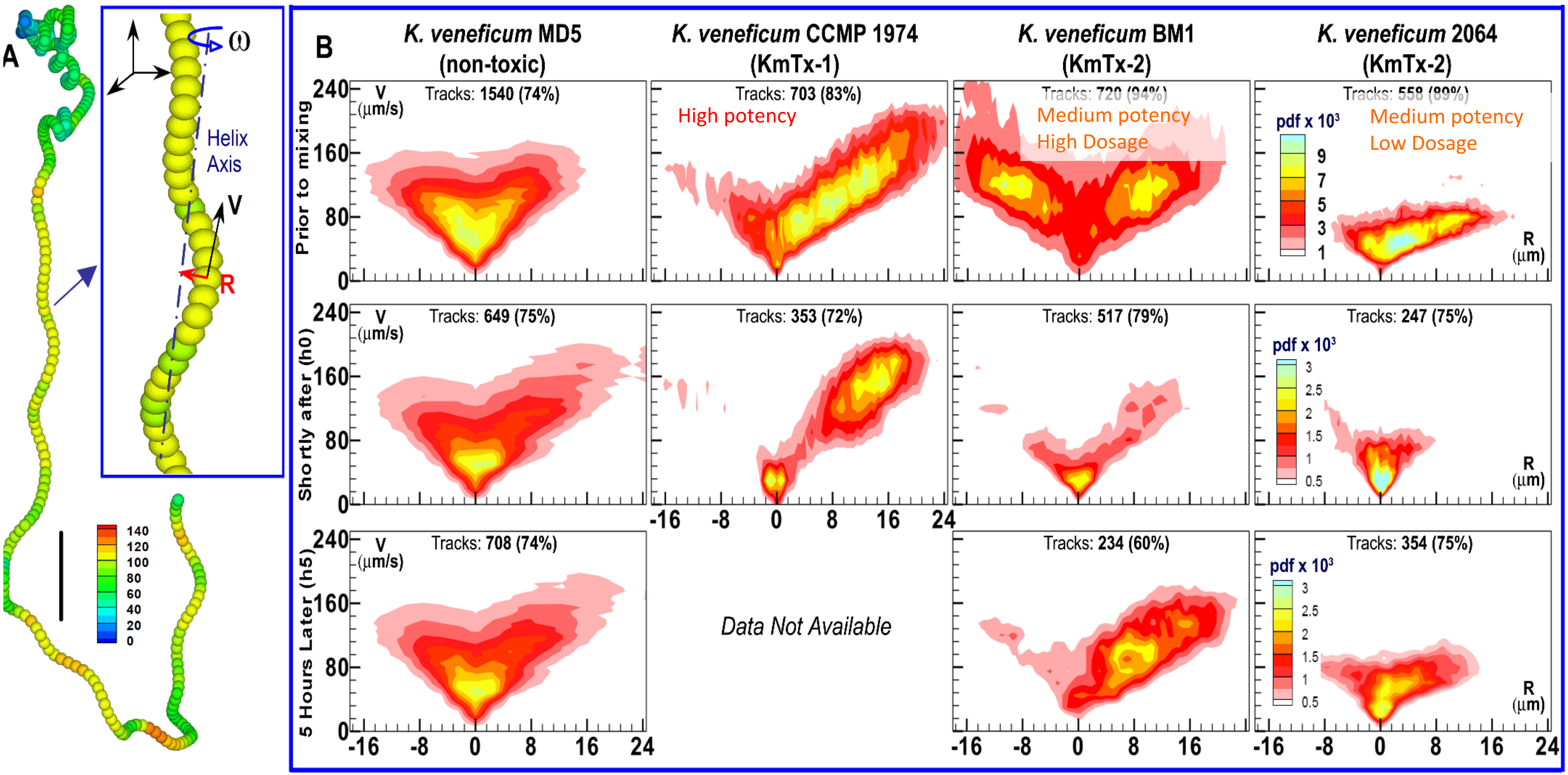

- All toxic (predatory) strains slow down in the presence of prey
- 1974 becomes bi-modal. 23% of the population slows down engaging in the process of ingesting prey.

Karlotoxins Immobilize Prey !

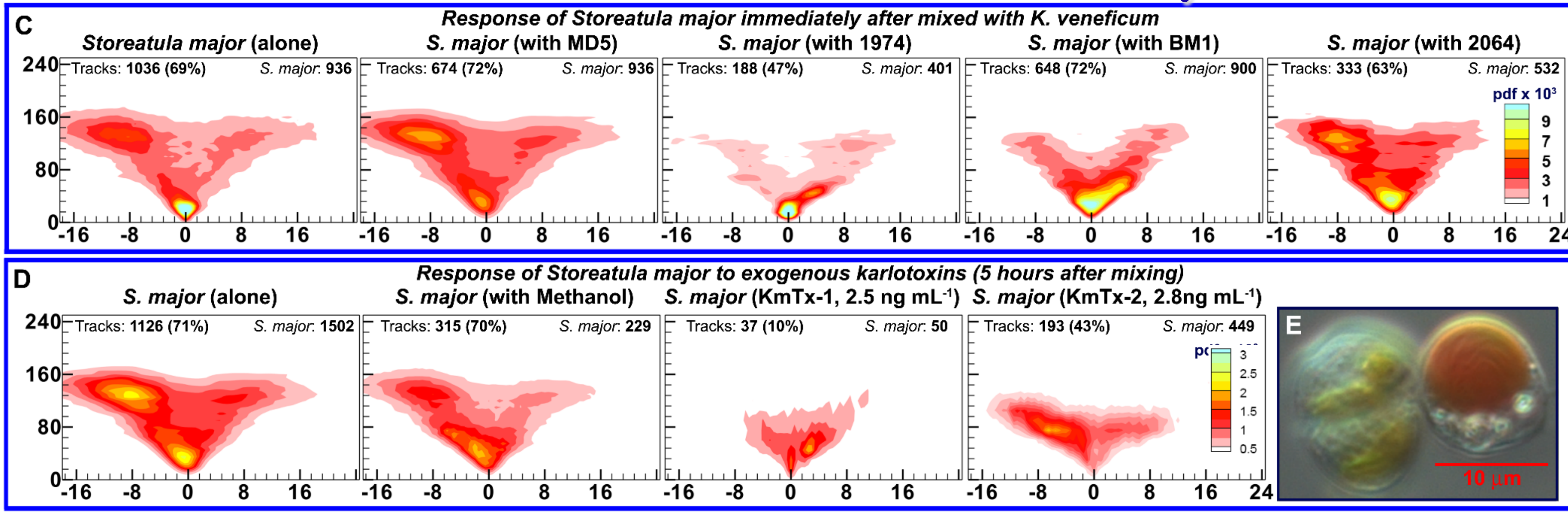

Fraction of immotile cells in suspensions

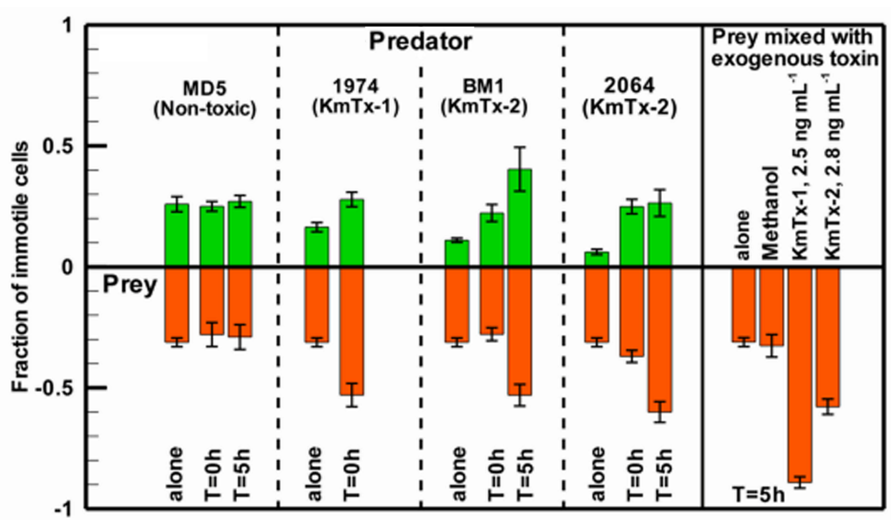

Karlotoxins immobilize prey

Swimming Induced Dispersion while intoxication

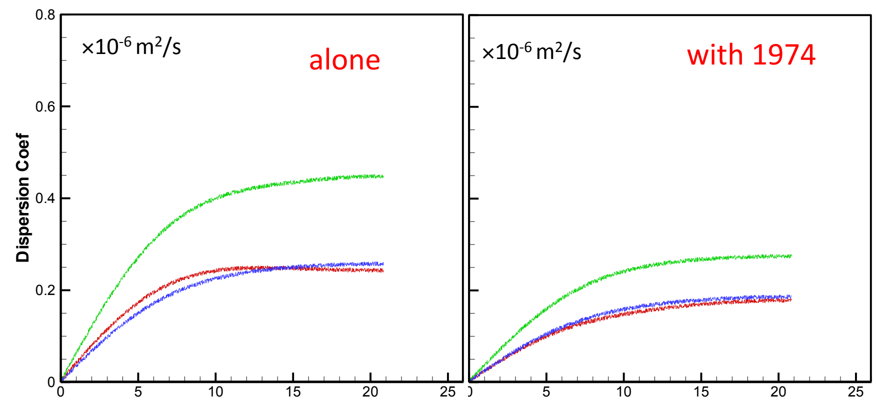

Karlotoxins slow down prey

Summary of Motilities of motile *K. veneficum* & *S. major*

Strain	*K. veneficum* (motile)					*S. major* (motile)				
	$V\pm\sigma_V$ ($\mu m/s$)	$R\pm\sigma_R$ (μm)	$\omega\pm\sigma_\omega$ (rad/s)	D_{zz}/ν	$D_{zz}/\bar{D}ii$ ($i=x,y$)	$V\pm\sigma_V$ ($\mu m/s$)	$R\pm\sigma_R$ (μm)	$\omega\pm\sigma_\omega$ (rad/s)	D_{zz}/ν	$D_{zz}/\bar{D}ii$ ($i=x,y$)
S. major						86.4±47.0	5.8±6.1	7.3±4.0	0.45	1.8
control *MD5*	81.3±44.9	4.57±4.9	6.98±3.7	2.67	9.1					
MD5 + S. major (h0⁺)	84.5±48.6	4.6±5.3	6.9±2.2	2.51	8.9	85.2±46.1	5.1±5.9	7.2±3.8	0.45	1.9
MD5 + S. major (h5⁺)	82.3±50.1	4.7±5.1	6.8±3.0	2.57	9.0	86.8±40.1	6.1±4.8	7.8±2.5	0.45	1.7
KmTx-1 *1974*	102.3±56.4	9.2±8.6	5.67±2.9	1.01	2.0					
1974+ S. major (h0)	160.4±59.6	16.2±5.7	8.7±6.1	0.85	1.6	42.7±37.7	2.9±4.3	8.1±4.1	0.28	1.5
KmTx-2 *BM1*	111.2±55.15	9.3±8.8	6.7±3.1	2.05	2.6					
BM1+ S. major (h0)	81.8±55.5	6.5±7.4	6.4±3.0	1.15	2.0	65.1±41.9	4.1±4.8	6.9±3.2	0.45	6.3
BM1+ S. major (h5)	92.7±43.6	8.7±7.5	5.6±2.7	1.28	2.5	69.8±44.6	5.1±6.0	6.7±3.3	0.5	1.7
2064	80.9±38.9	6.5±6.8	5.0±2.7	0.78	3.2					
2064 + S. major (h0)	37.8±40.1	3.76±5.0	6.8±3.8	0.64	3.1	81.7±44.4	4.7±5.2	6.9±3.5	0.72	4
2064+ S. major (h5)	59.4±35.1	4.7±5.1	5.5±3.0	0.61	3.1	63.2±41.4	4.2±5.6	6.4±3.0	0.25	1.4

KmTx-1 Producing Strain

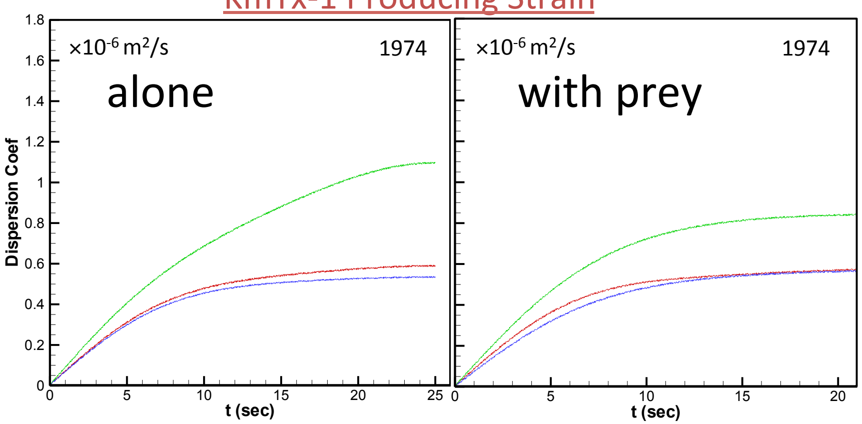

KmTx-2 Producing Strain

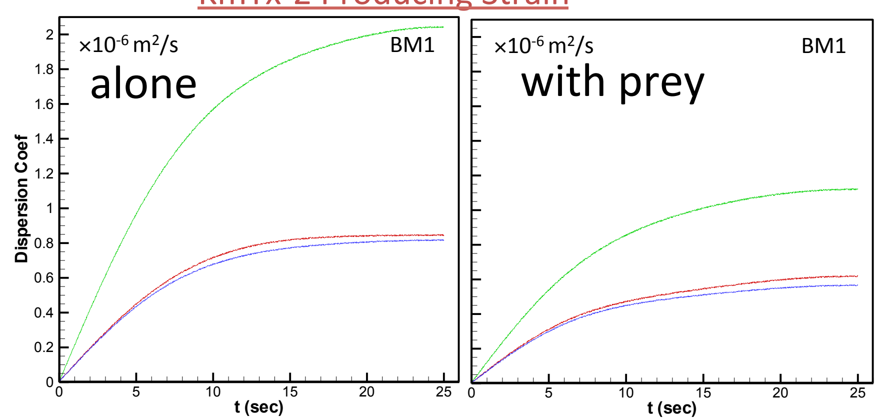

Conclusion

Karlotoxins serve as a prey capturing instrument
predation promotes *mixotrophic growth*

Future Questions

- How are toxins delivered – direct contact or close proximity?
- What are the effects of environmental factors; turbulence, shear, etc?
- Is the observed function universal in mixotroph?

Study II: Flow Shear Induced Crossstream Migration by a Green Algae – Potential Mechanism for Thin Layer Formation and Harvest






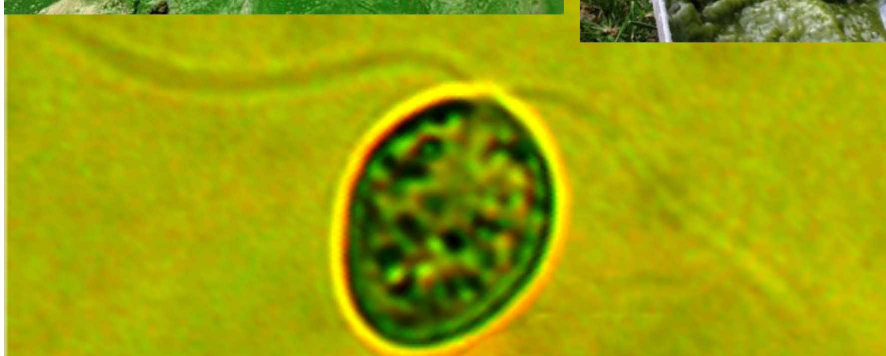


Flow Environment: Shear Flows in μFluidics

Velocity Profile in the μFluidic Channel

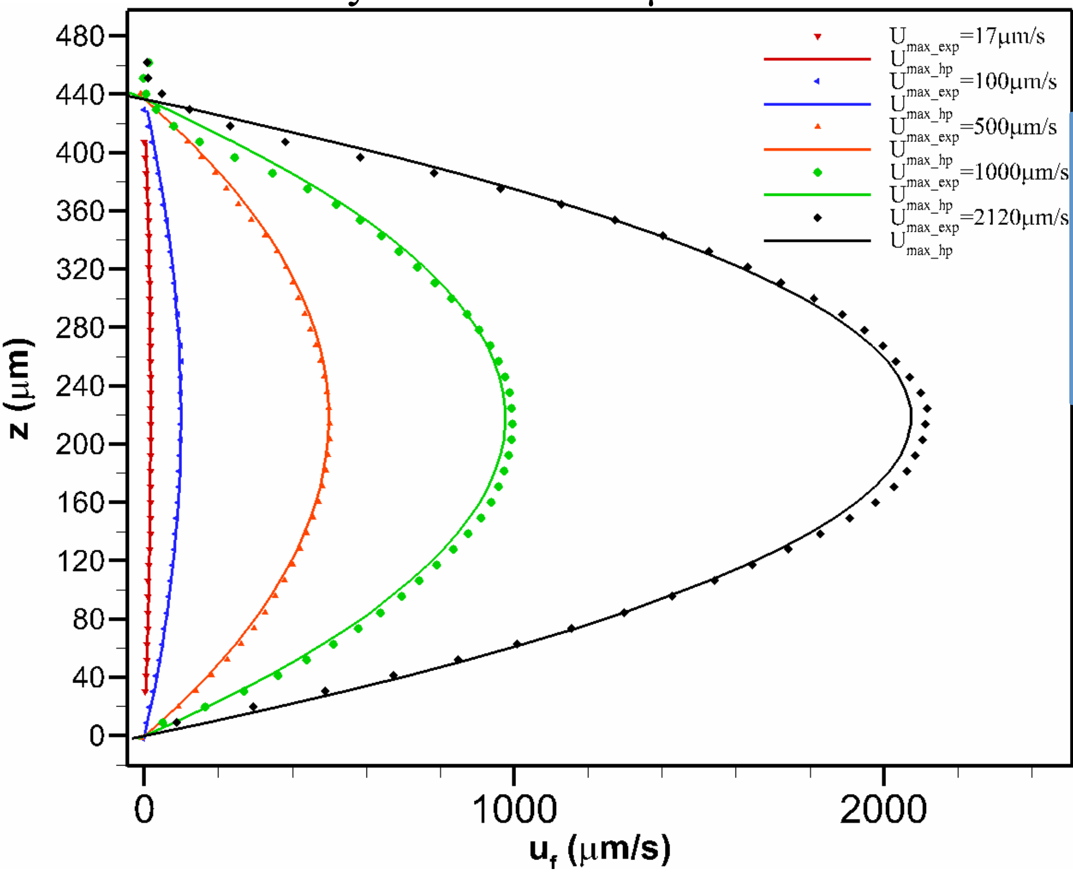

U_{max} (μm/s)	dU/dz (1/s)	# of tracks obvserved	Cell density 10^6 (cell/ml)
No flow	0	283	
17	0.15	267	
100	1	767	3.6
500	5	954	
1000	10	1303	
2120	20	1325	

Hagen-Poiseuille Flow in a rectangualar micro-channel solved using Fourier series

$$v(x\ ,y\ )=\frac{\Delta p}{\eta L}\frac{4h^2}{\pi^3}\times\sum_{n=1,3,5....}^{\infty}\frac{1}{n^3}\left(1-\frac{\cosh(n\pi\ x/h)}{\cosh(n\pi\ w/2h)}\right)\sin(n\pi\ y/h)$$

Steady state flow in a channel with large cross-sectional aspect ratio:

$$\boxed{u=\frac{6\,Q\,(hz-z^2)}{h^3}}$$

Surface plot

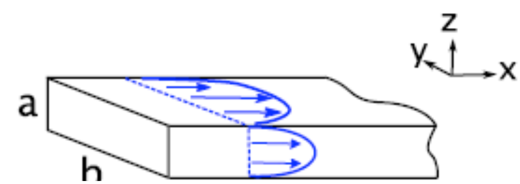

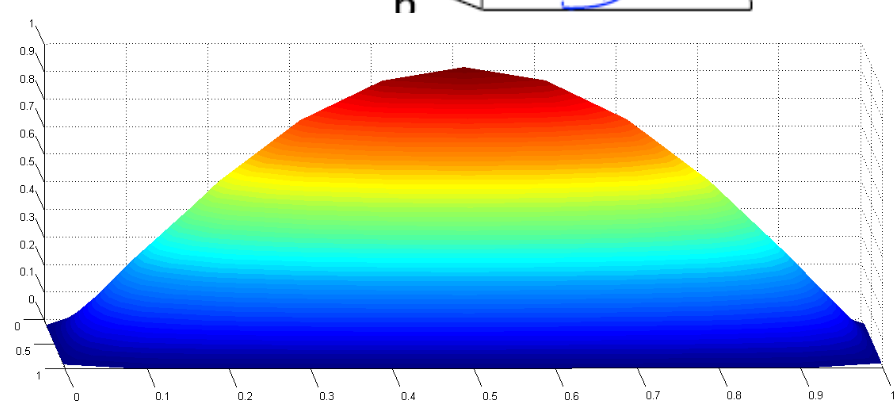

Overlapped In-focus Cell Images over Entire Depth (No shear)

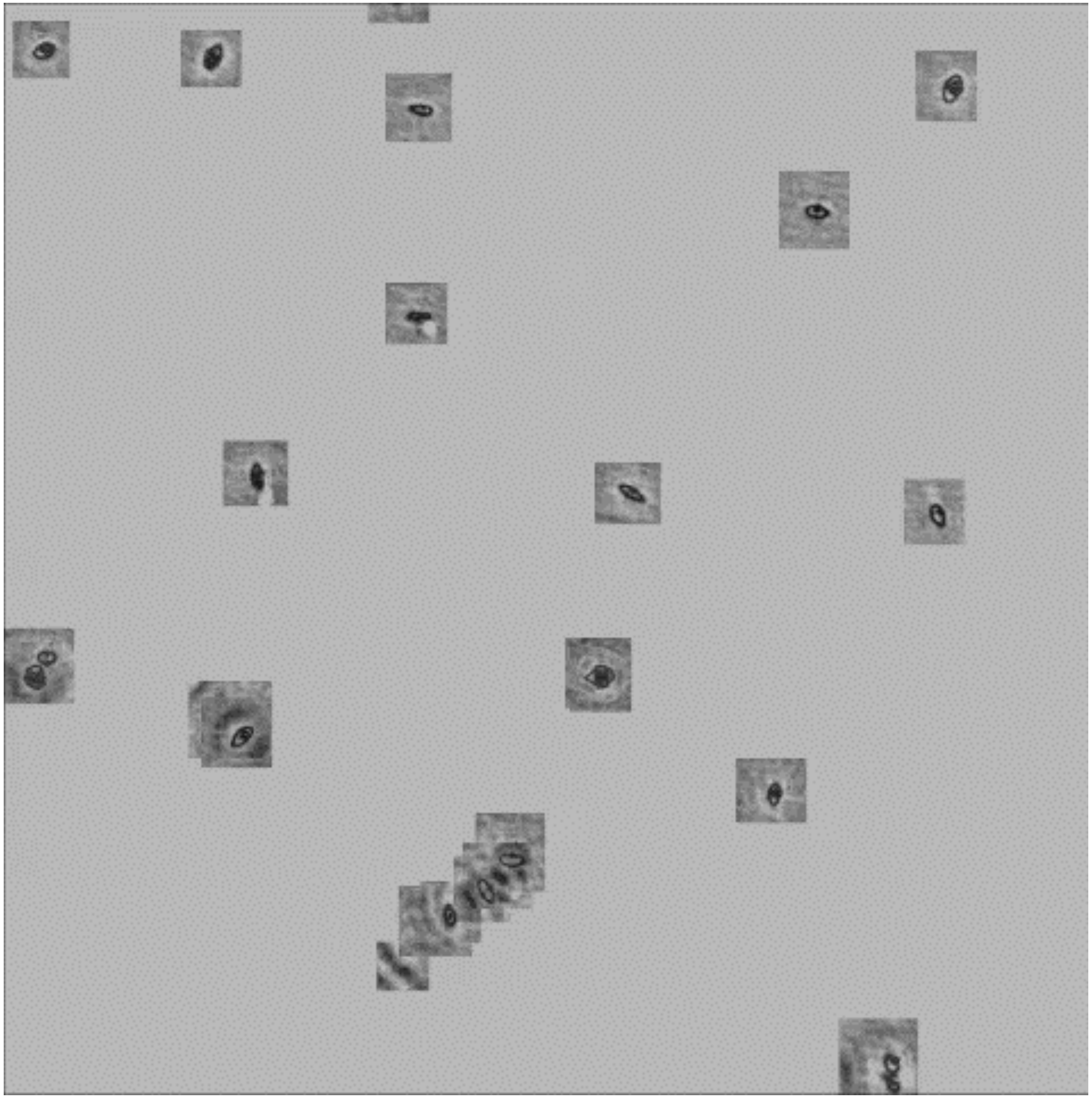

Close-up of *Dunaliella*

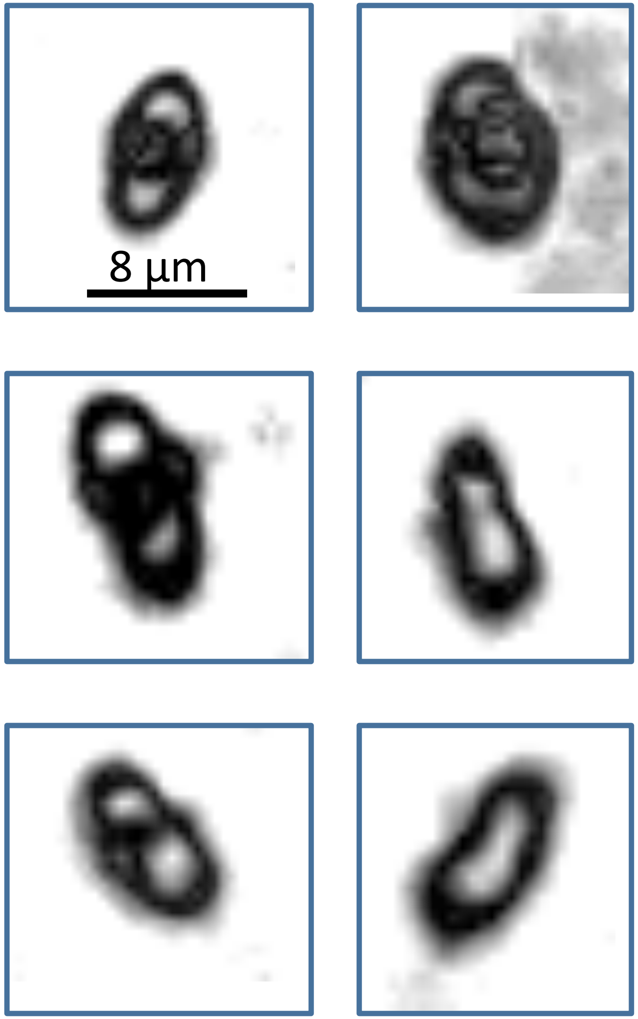

Rheotaxis Behavior Observed at Higher Flow Shear (>30 1/s)

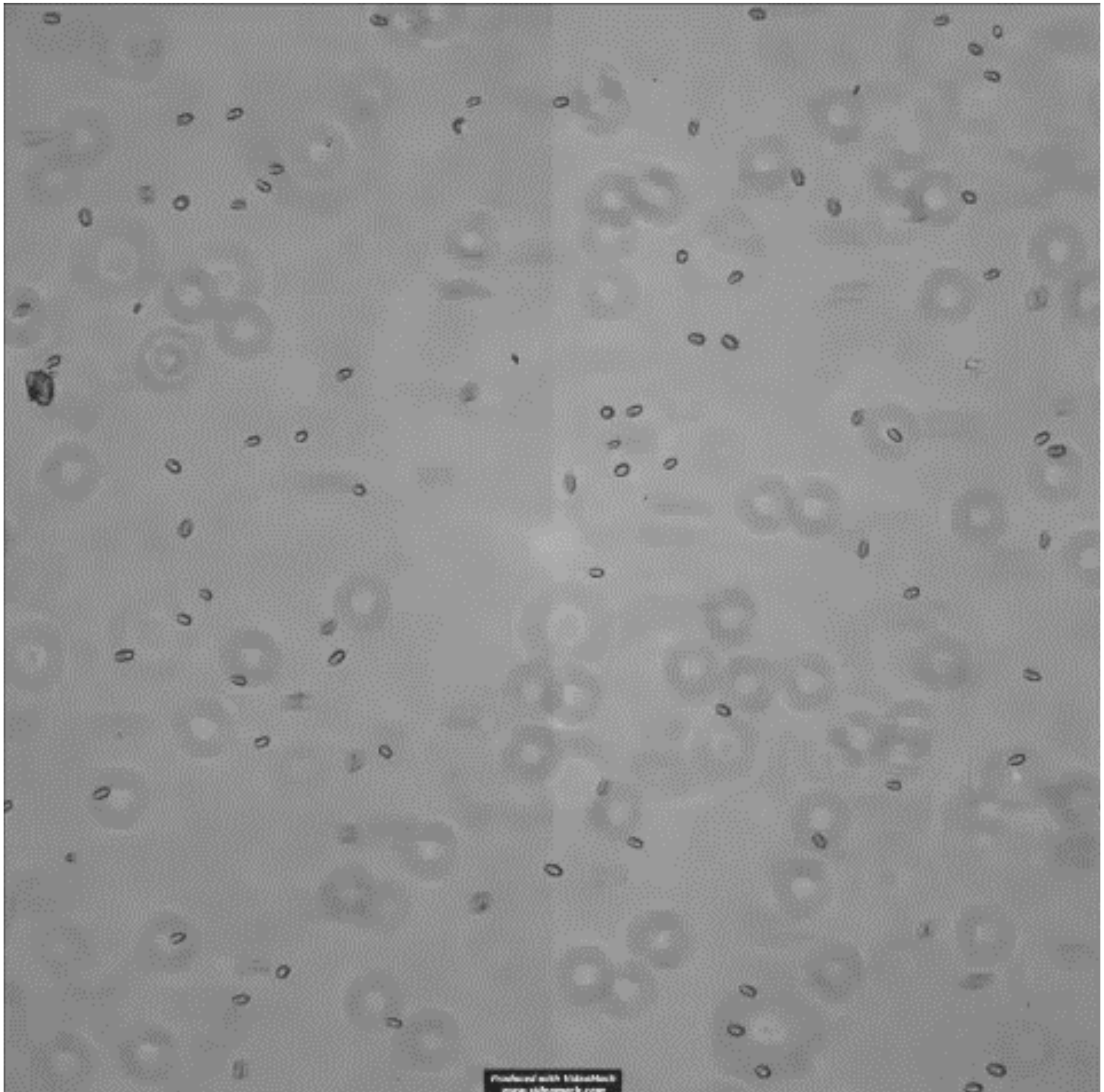

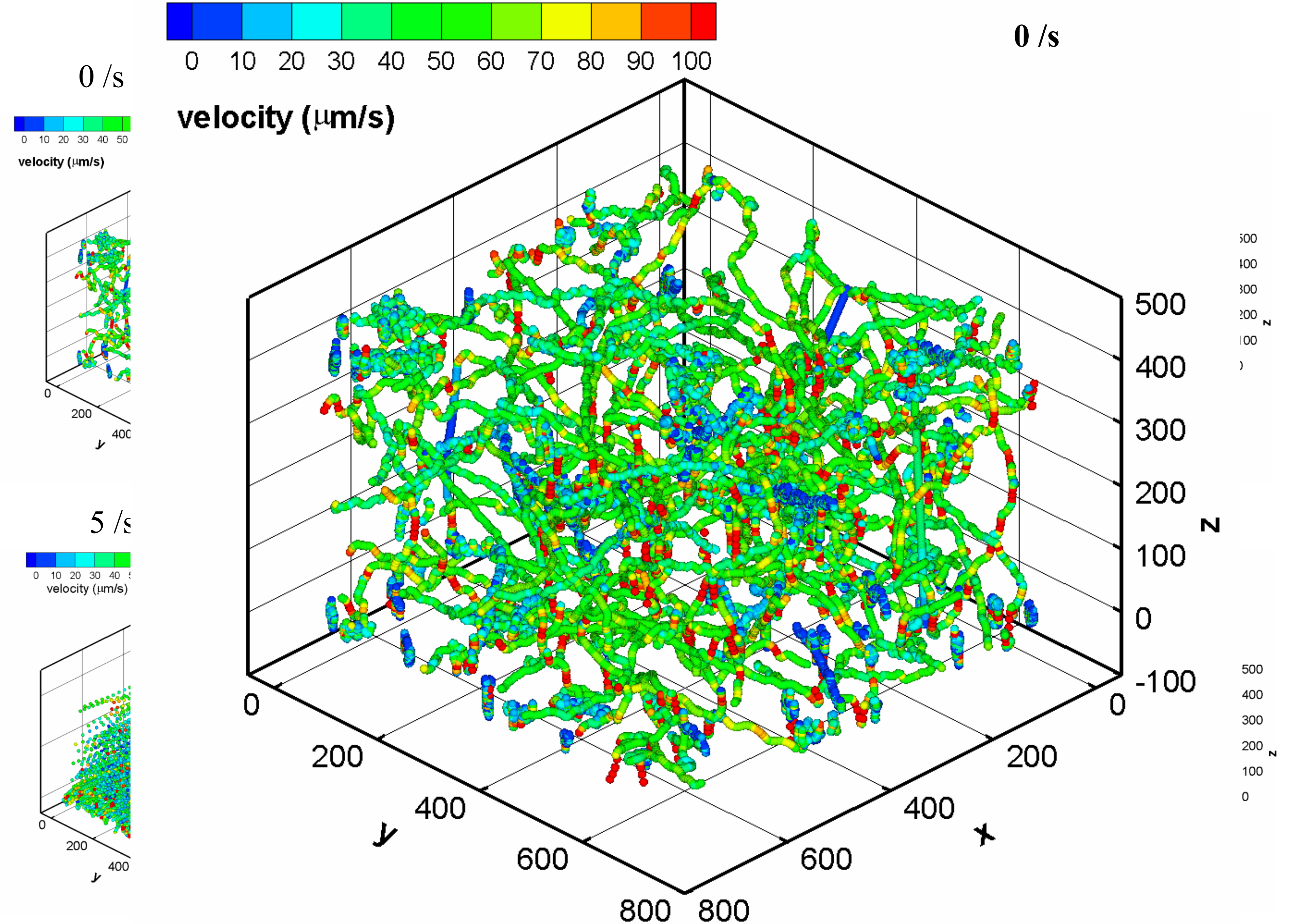

All dimensions are in microns

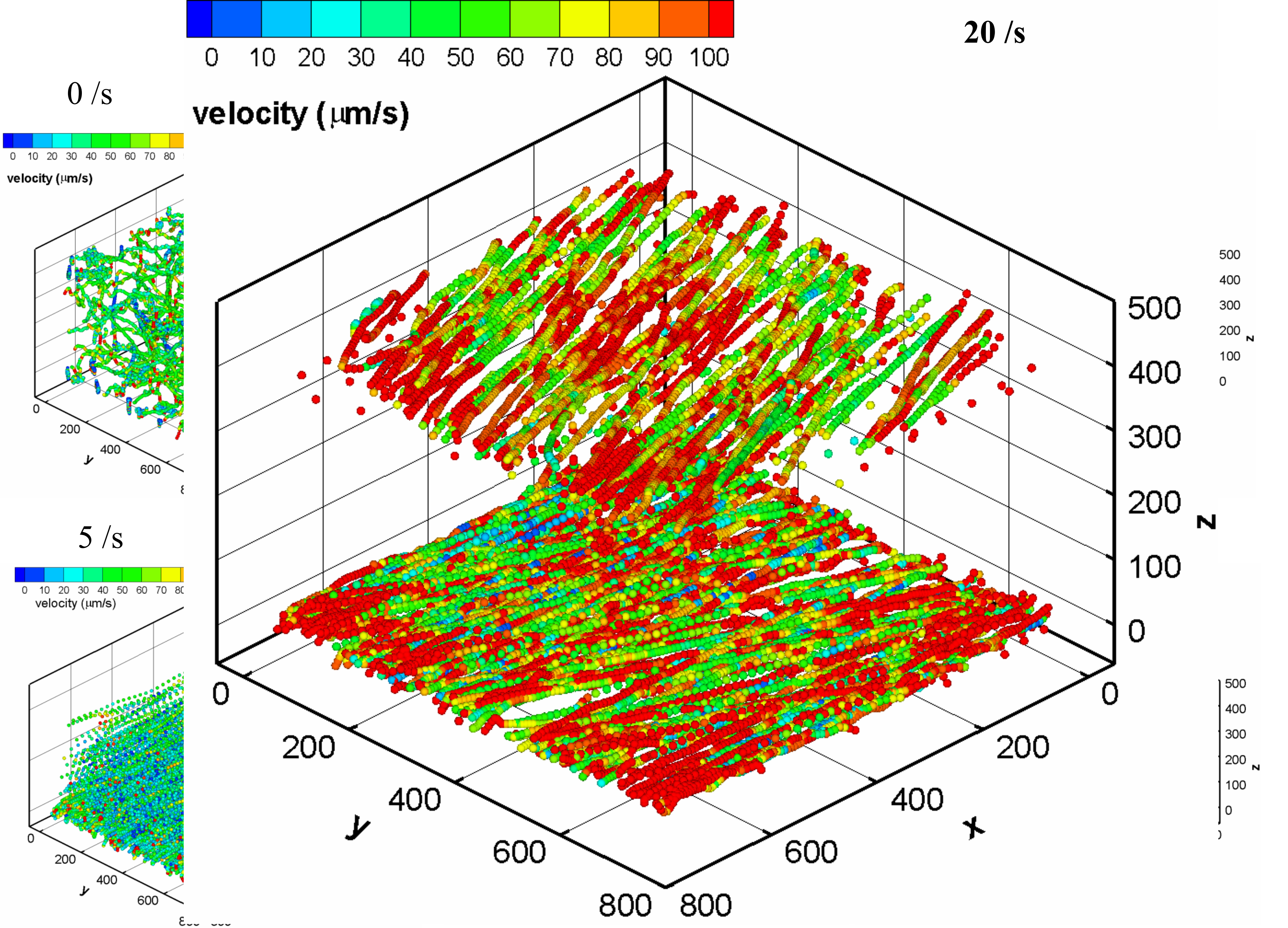

All dimensions are in microns

Prevalent Rheotaxis of Microbes in a Shear Flow: microalgae surfs along flow vortices

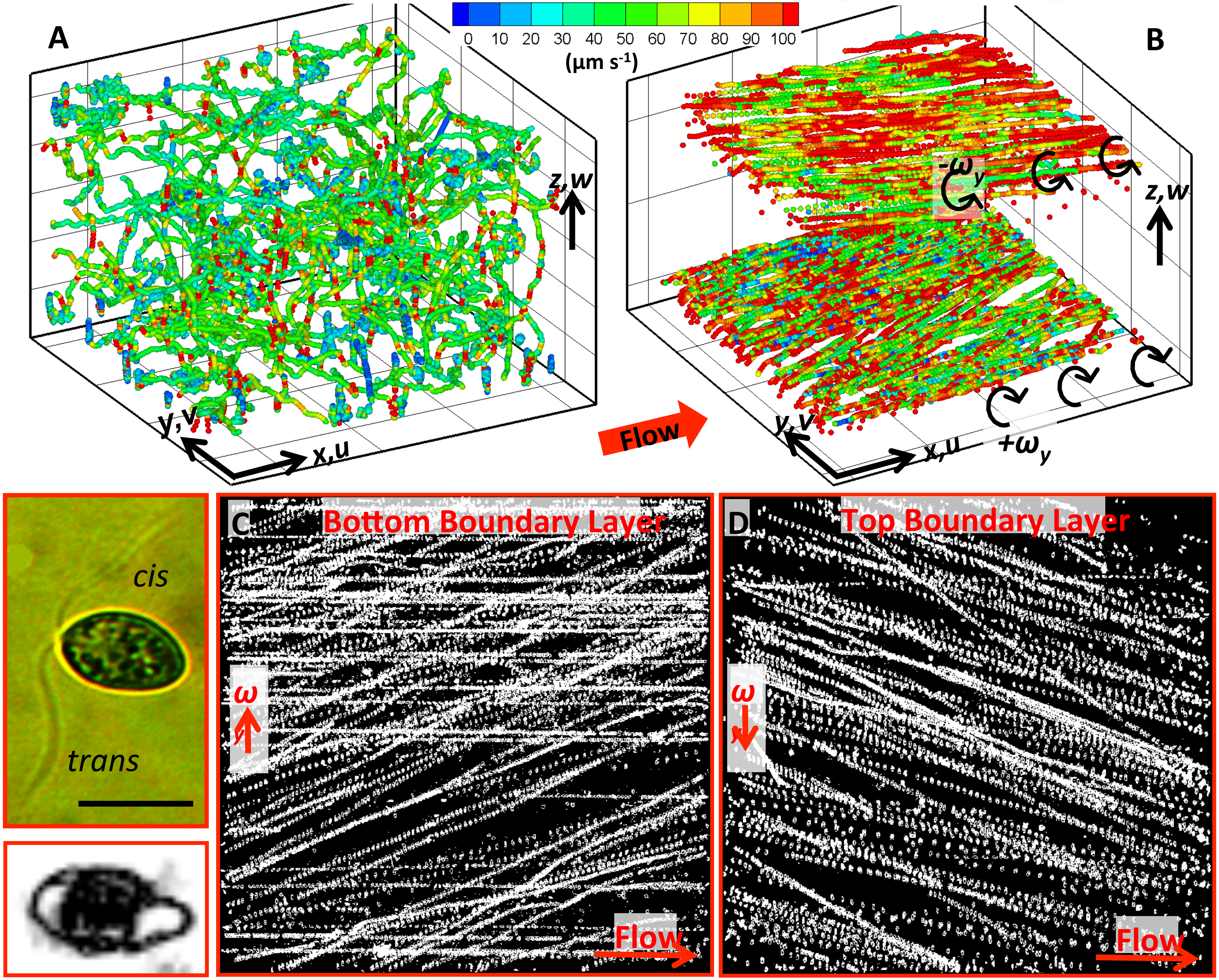

Histogram of Swimming Velocities of *Dunaliella*

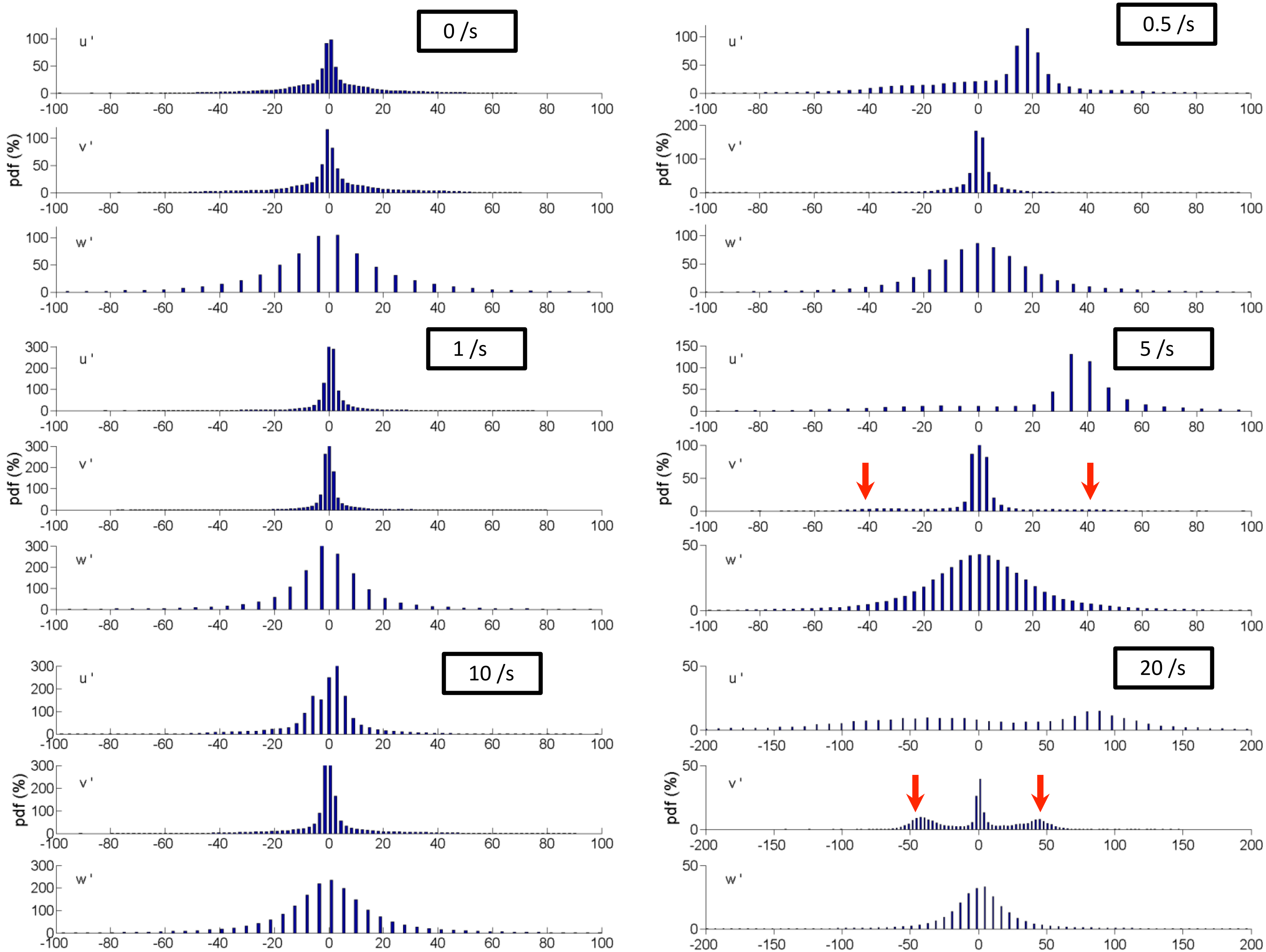

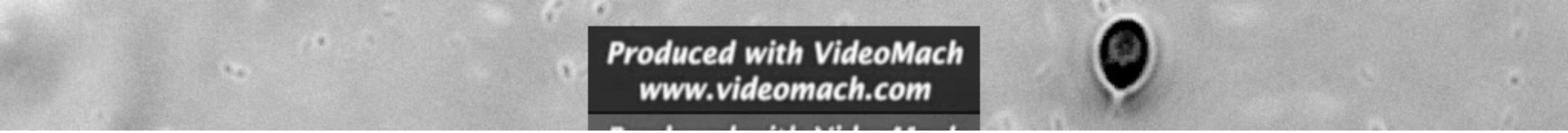

Jeffrey Orbits

Passive Spheroids immersed in a viscous shear flow undergo periodic motion

Mason & Manley, 1956

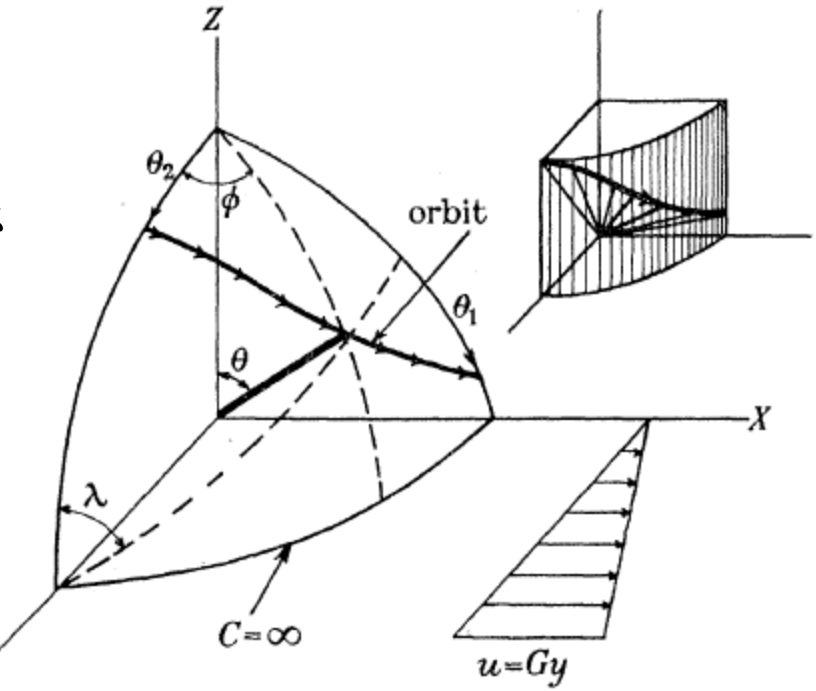

$$T = \frac{2\pi}{G}\left(r_e + \frac{1}{r_e}\right)$$

$$\tan^2\theta = \frac{a^2b^2}{k^2(a^2\cos^2\phi + b^2\sin^2\phi)},$$

$$\omega(\phi) = \frac{G}{(r_e^2+1)}[r_e^2\cos^2\phi + \sin^2\phi],$$

$$p(\phi) = \frac{r_e}{2\pi(r_e^2\cos^2\phi + \sin^2\phi)}.$$

0.90 s

Fixed algae

Microalgae under Shear Does Not Reorient and Disperse as Passive Particles

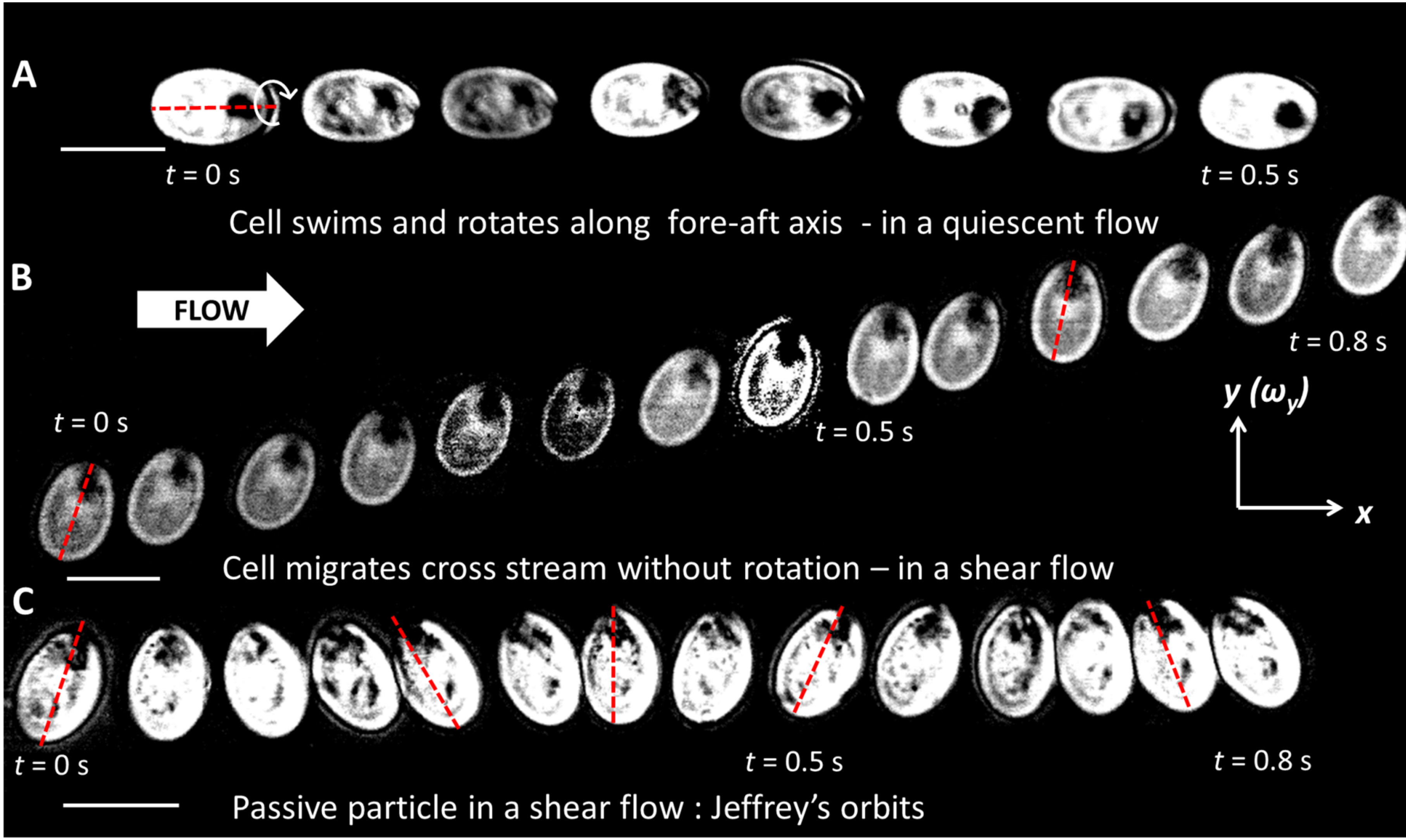

Anwar, Hondzo and Sheng, PRE, 2013

Further Evidence Rheotaxis

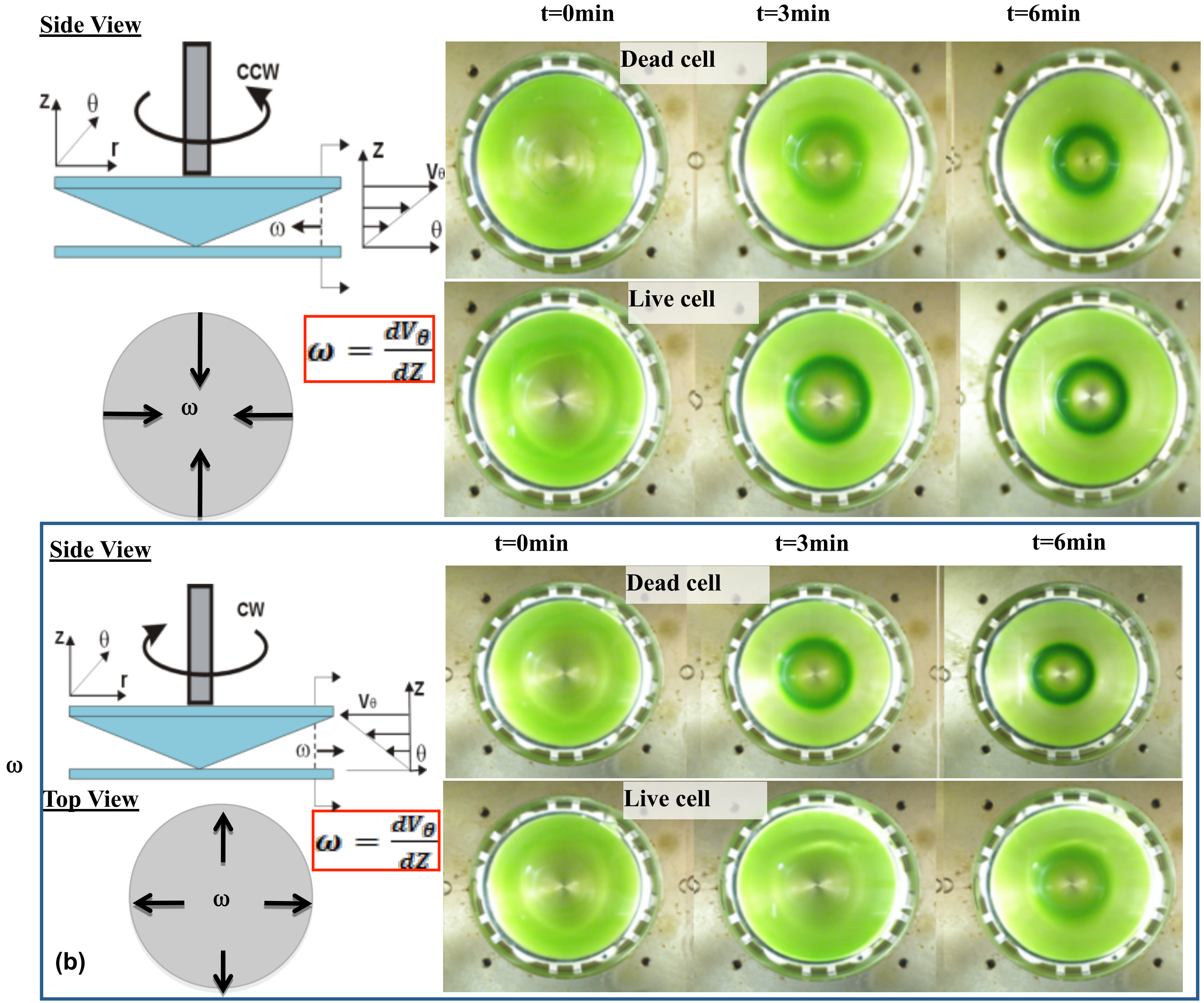

Anwar, Hondzo and Sheng, PRE, 2013

Dispersion

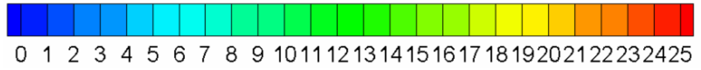

0 1 2 3 4 5 6 7 8 9 10 11 12 13 14 15 16 17 18 19 20 21 22 23 24 25

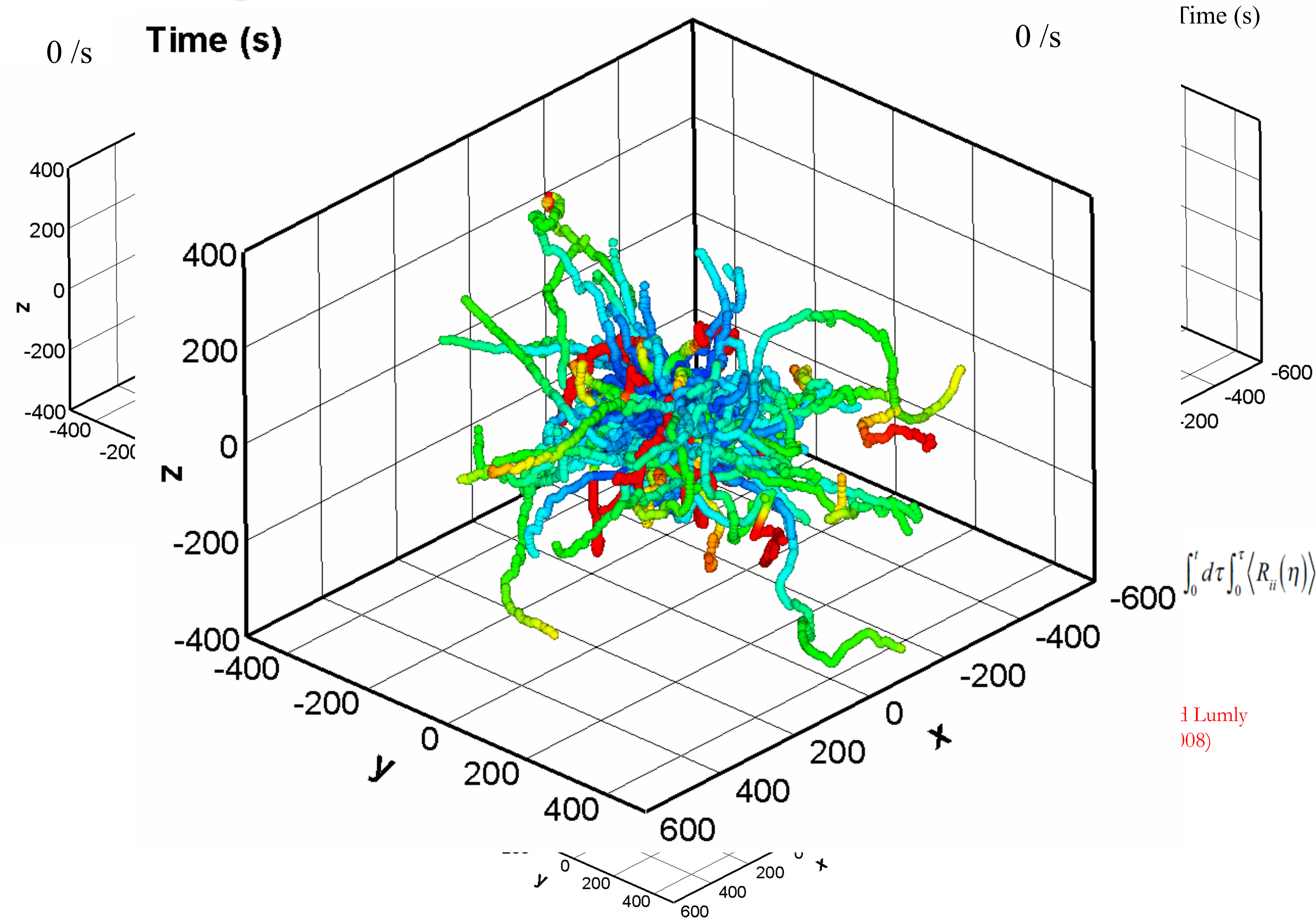

Time (s)
0 /s
400
200
0
-200
-400
z
-400
-200
0
200
400
600
y
-600
-400
-200
0
200
400
x

Dispersion

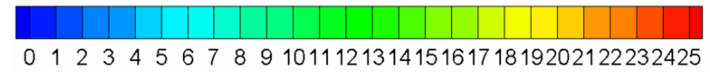
0 1 2 3 4 5 6 7 8 9 10 11 12 13 14 15 16 17 18 19 20 21 22 23 24 25

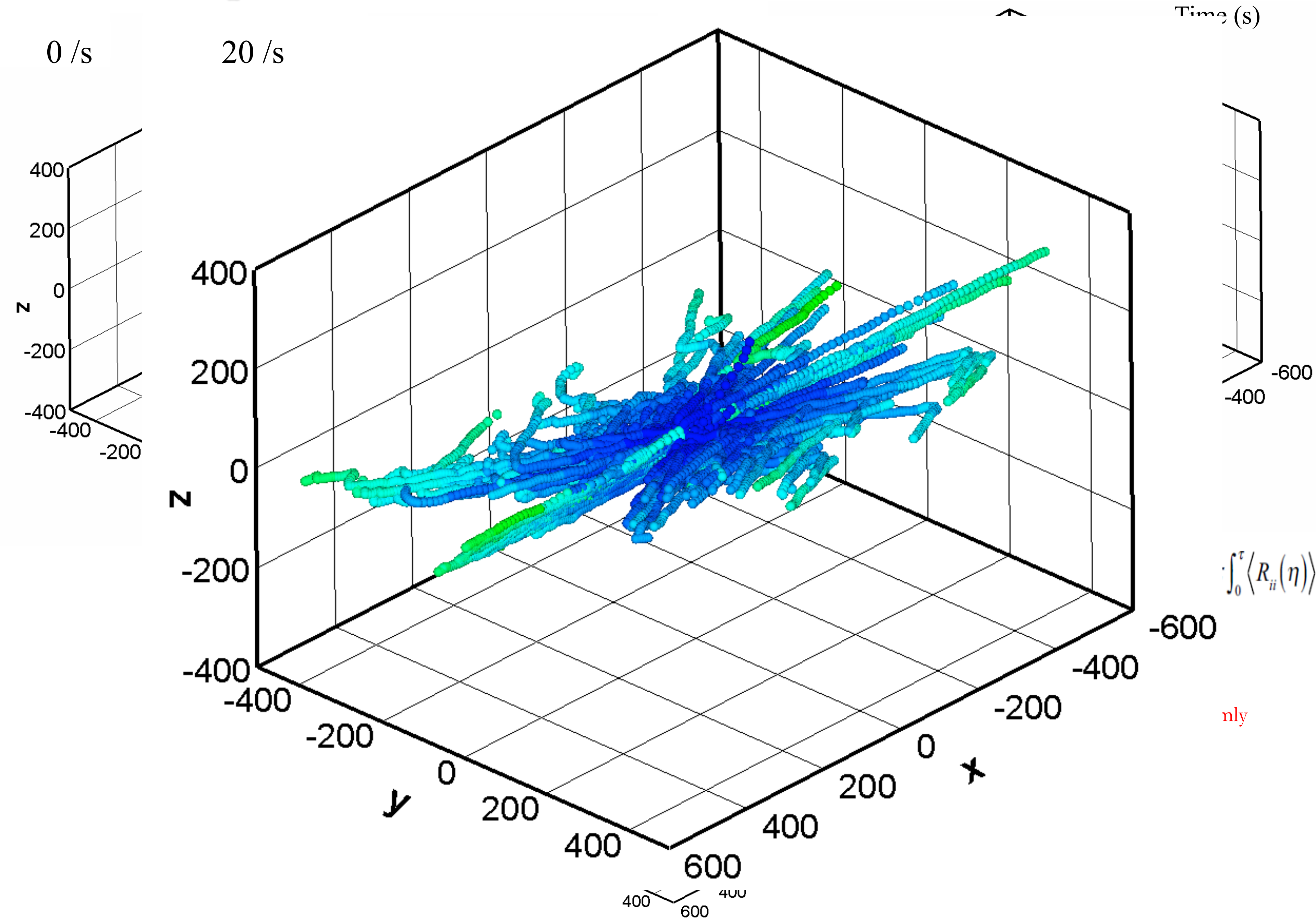
Time (s)
0 /s
20 /s
400
200
0
-200
-400
z
y
x
-400
-200
0
200
400
600
-600
nly

Effects of Rheotaxis on Dispersion

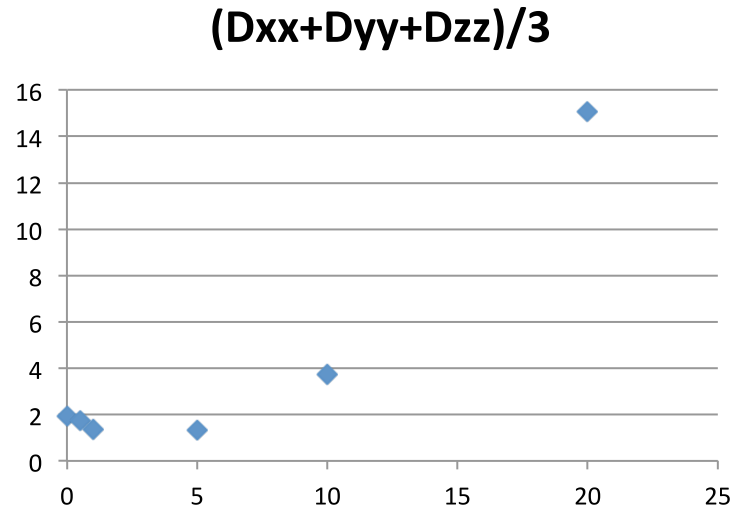

Dispersion coefficient determined from Lagrangian velocity autocorrelation functions

$$D_{ii}(t)=\left\langle \int_0^t d\tau \int_0^\tau R_{ii}(\eta)\,d\eta \right\rangle = \int_0^t d\tau \int_0^\tau \left\langle R_{ii}(\eta)\right\rangle$$

Taylor (1921), Snyder and Lumly (1971), Gopalan et al. (2008)

Flow shear increases isotropic dispersion tensor $\frac{1}{3}D_{ii}$

Flow shear increases shape of anisotropic dispersion

$$D_{ij}-\frac{1}{3}D_{kk}\delta_{ij}$$

1 Sphere

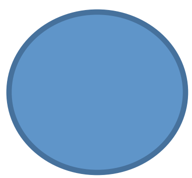

2 Axisymmetric cylinder

3 Thin slice

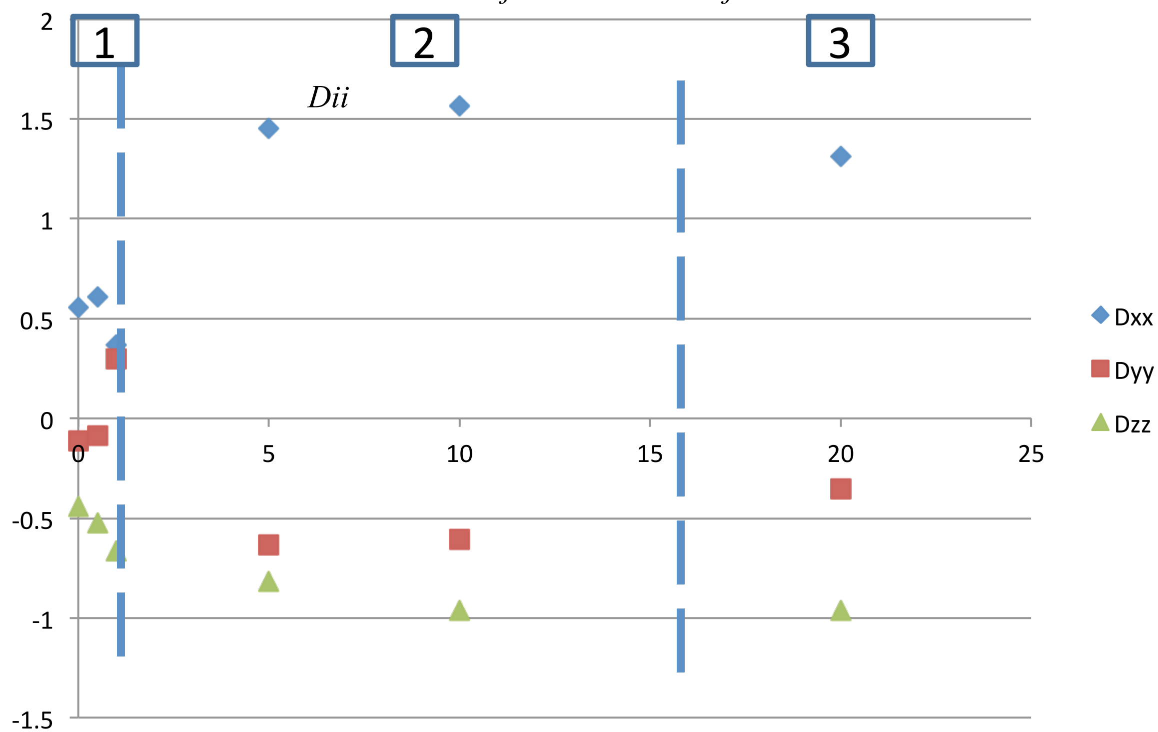

Study III: Escape Kinematics of a Nauplius at Various Temperature

Temperature changes viscosity that affect effectiveness of swimming

Experimental Setup

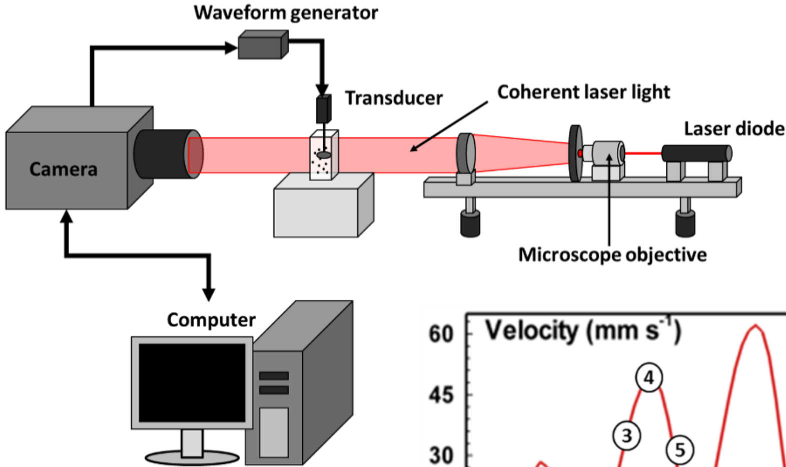

Objective and Motivation

- *In-situ* measurement of escape kinematics of *A. tonsa* Nauplius under different temperatures
- Understand the biophysical interactions between temperature induced viscosity change and the escape effectiveness
- Understand the evolutionary fitness of organisms

Gemmell B., Sheng. J, PNAS 2013

- High speed recording at 2000 fps
- 3D holographic microscopic imaging at 4X magnification
- Numerical simulation using Resistance Force Theory for modeling
- Discovery new compensatory mechanism

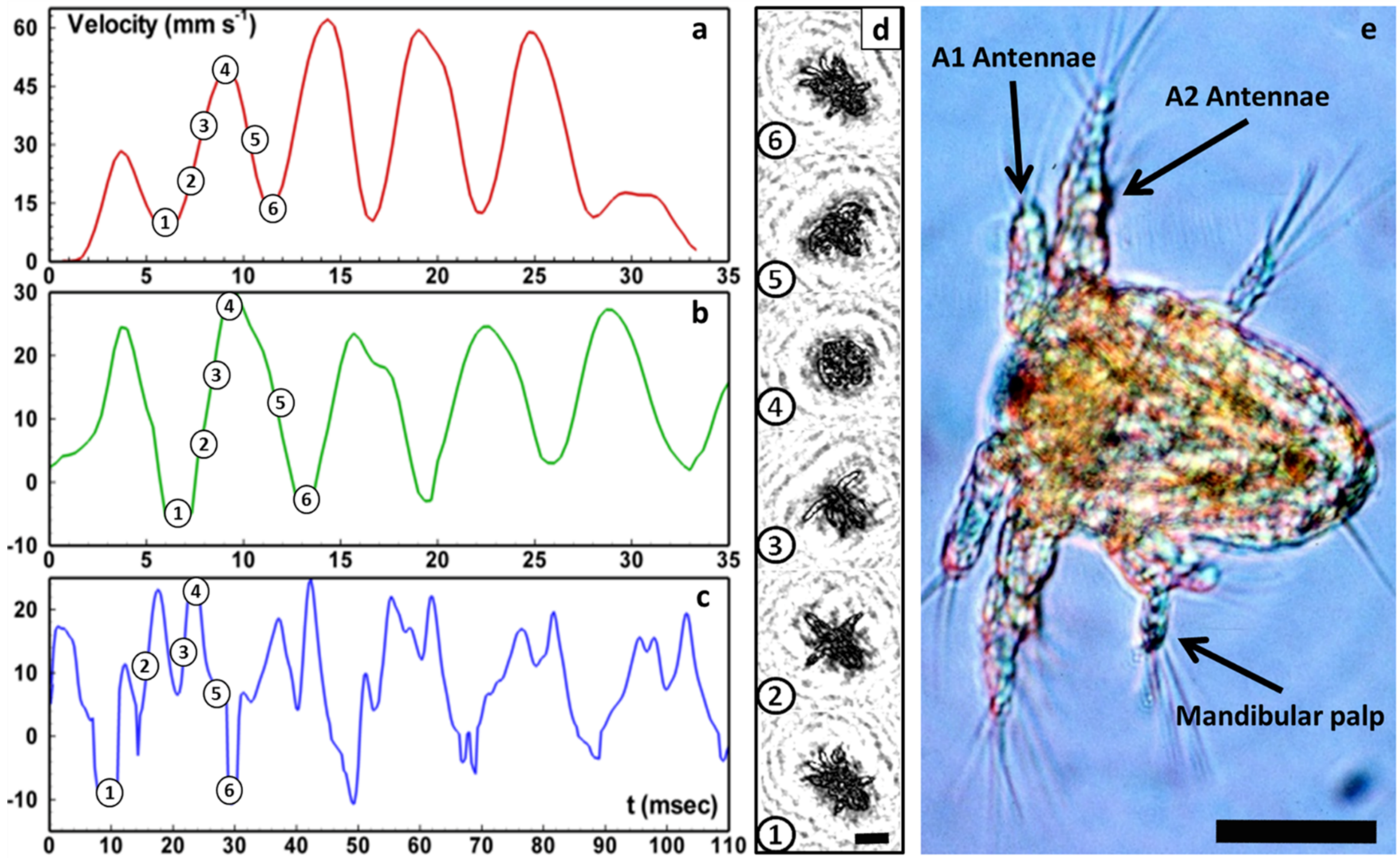

Gemmell B., Sheng. J, et al. PNAS 2013

Escape Characteristics & Compensatory Mechanism

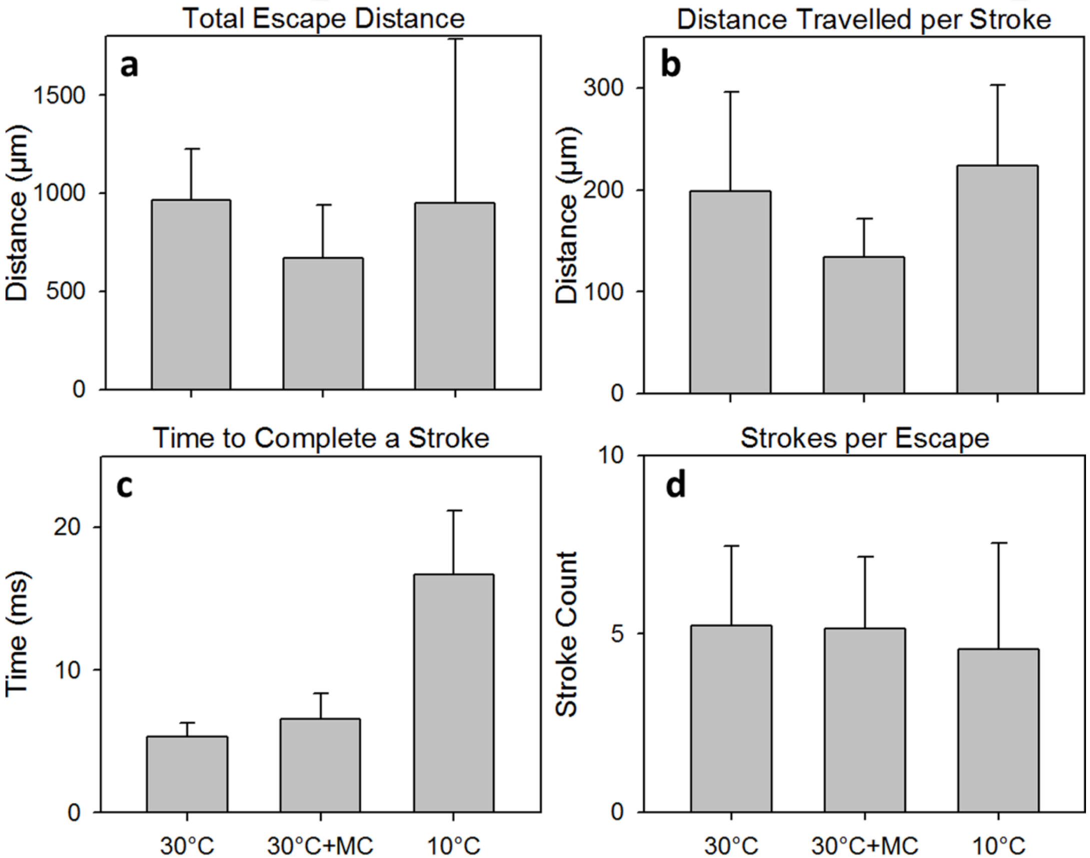

Appendage Kinematics

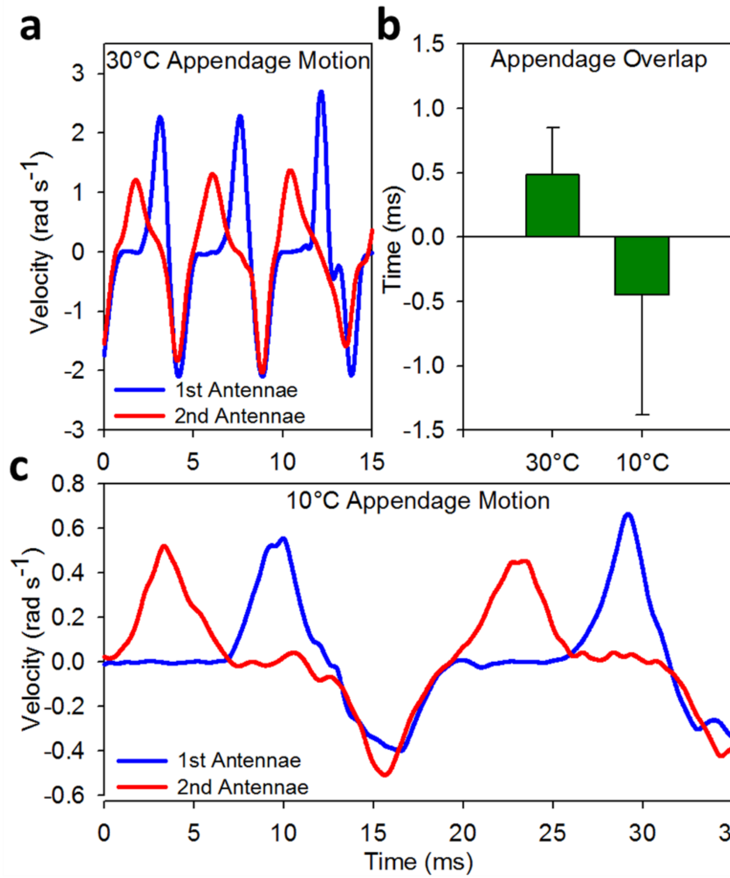

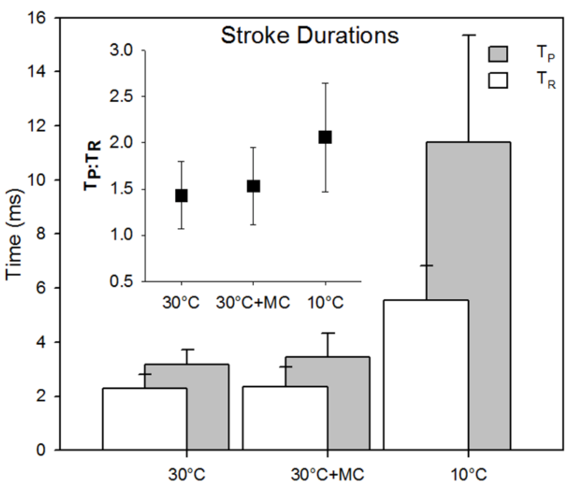

- Temperature induced viscosity does not affect the escape distance, but the viscosity increase as the fluids property does
- Strokes show clear overlap in high temperature but low viscosity, but reduced the overlap in low temperature but high viscosity.
- Viscosity change alone does not trigger the change in escape kinematics

Gemmell B., Sheng. J, et al. PNAS 2013

Resistance Force Modeling

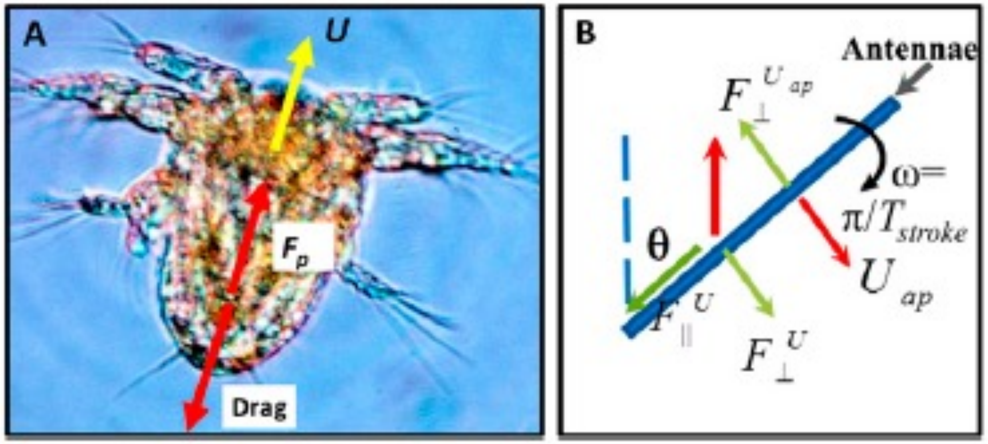

Kinetics of appendages: propulsion force, F_p

Propulsion Force using RFT

$$\boxed{F_p = F_{V_\perp} \cos\theta - F_{V} \ldots}$$

Resistance Force Theory (Re ~ 1)

$$F/8\pi\mu V^r L = \varepsilon - 0.193\varepsilon^2 + 0.215\varepsilon^3 + 0.97\varepsilon^4 + \ldots$$

Linear Model (Re < 1)

$$F_{V_\perp} = 4\varepsilon_\perp \pi\mu V_\perp L_{ap}, \quad F_{V_\parallel} \ldots$$

$$\varepsilon_\perp = [\ln(4L_{ap}/b_{ap})]^{-1}, \quad \gamma = \varepsilon_\parallel \ldots = 1.8\sim 2$$

$$\boxed{F_p = -4\pi\varepsilon_\perp \mu L_{ap}[2U(\sin^2\theta + 1/\gamma \cos^2\theta) + \omega L_{ap} \sin\theta]}$$

Nonlinear Model (Re > 1)

$$F_{V_\perp} = 4(\varepsilon_\perp + C_{1,\perp} V_\perp^r)\pi\mu V_\perp L_{ap}$$

$$F_{V_\parallel} = 4(\varepsilon_\parallel + C_{1,\parallel} V_\parallel^r)\varepsilon_\parallel \pi\mu \ldots$$

$$\boxed{-4\pi\varepsilon_\perp \mu L_{ap}[2U(\sin^2\theta + 1/\gamma \cos^2\theta) + \omega L_{ap} \sin\theta] - 4\pi C_{1,\perp}\mu L_{ap}[2U^2(\sin^2\theta + 1/\gamma \cos^2\theta) + 1/2\,\omega^2 L_{ap}^2 \sin\theta]}$$

Equation of motion $(m_p + 1/2\, m_f) dU/dt = F_{prop} - F_{drag} + F_{other}$

Body Drag Force (Re >>1) $Drag = 1/2\, \pi C_D \rho_f R^2 U^2$

where $C_D = 24\cdot Re^{-1} + 5\cdot Re^{-1/2} + 0.4$, $Re = 2RU/\nu$

Dynamic Escape Model

$$\boxed{2\pi R^3 \rho_f\, dU/dt = F_p - 6\pi\mu RU - 5\pi(2^{-3}\rho\mu R^3 U^3)^{1/2} - 1/5\, \pi\rho R^2 U^2}$$

Kinetic Simulations:

$$dX_p/dt = U$$

$$2\pi R^3 \rho_f\, dU/dt = F_p(U, \theta_1, \theta_2, \theta_{12}) - 6\pi\mu RU - 5\pi(2^{-3}\rho\mu R^3 U^3)^{1/2} - 1/5\, \pi\rho R^2 U^2$$

$$d\theta_1/dt = -\omega_{ap} G(t - t_1, \ldots$$

Table S1. Physiological parameters used in numerical simulations

Parameters	30 °C Power	30 °C Recovery	10 °C Power	10 °C Recovery	30 °C + MC Power	30 °C + MC Recovery
Simulation parameter						
Kinematic viscosity, ν $(m^2 \cdot s^{-1})$	0.84×10^{-6}		1.34×10^{-6}		1.34×10^{-6}	
Appendage parameter						
Length, L_{ap} (μm)			54.6 ± 1.1			
Width, b_{ap} (μm)	28.9 ± 0.7	4.8 ± 0.3	28.9 ± 0.7	4.8 ± 0.3	$28.9 + 0.7$	4.8 ± 0.3
Stroke duration, T_{ap} (ms)	2.1 ± 0.6		5.1 ± 0.9		2.3 ± 0.4	
$Re_{ap} = \omega_{ap} L_{ap} b_{ap} / \nu$	2.8	0.47	0.44	0.08	2.6	0.4
$\varepsilon = \ln^{-1}(4L_{ap}/b_{ap})$	0.49	0.261	0.49	0.261	0.49	0.261
Cell body parameter						
Equivalent radius, R (μm)			50			

Mean statistics are averaged over ~30 samples per experimental condition and accompanied by SDs.

Simulation Results

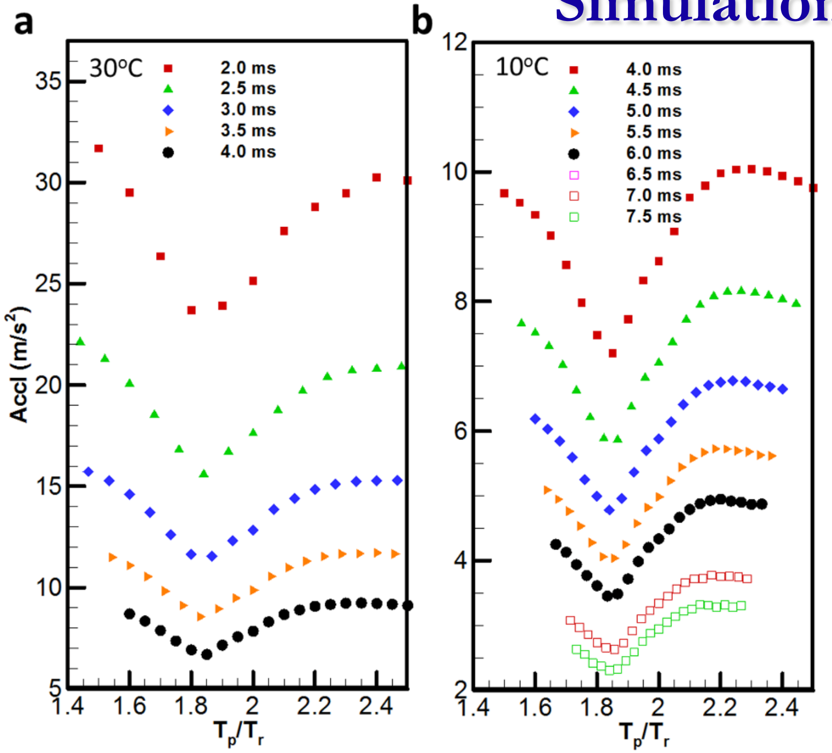

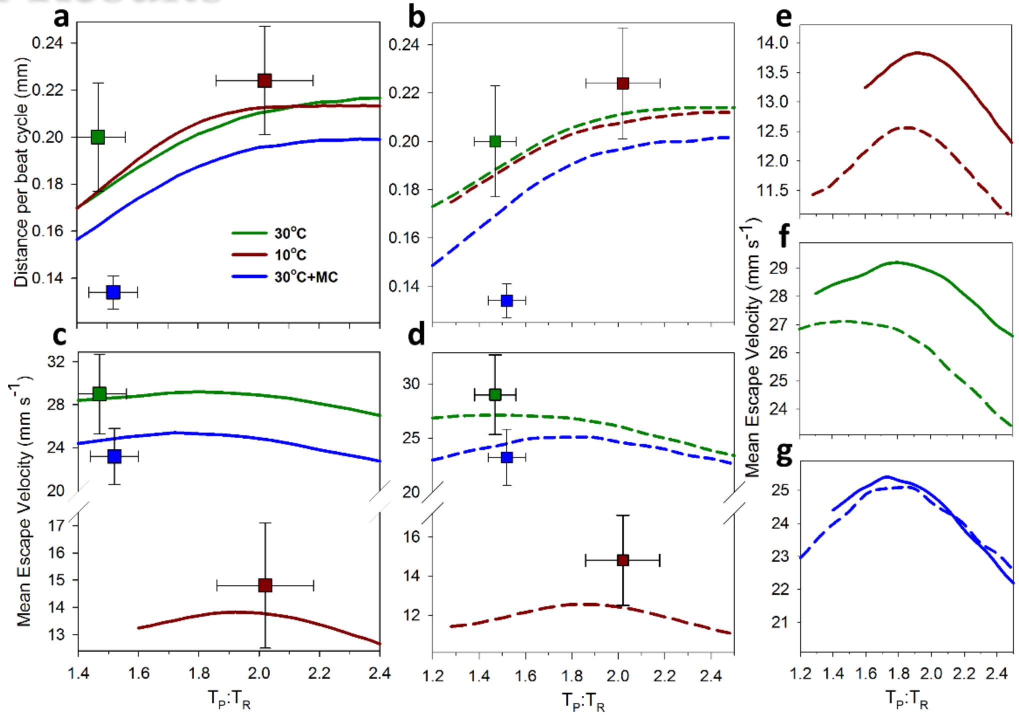

Experimentally measured mean velocity compared with model results

	Mean velocity, mm·s⁻¹			% difference	
Parameters	Experimental	RTF model	Nonlinear model	Experimental vs. RTF model	Experimental vs. nonlinear model
30 °C	29.5 ± 7.0	28.6	27.1	3.1	8.1
30 °C+MC	23.2 ± 6.6	25.0	24.5	7.8	5.6
10 °C	15.0 ± 5.0	13.8	12.5	8.0	16.7

Experimentally measured T_P/T_R compared with model results

	T_P/T_R			% difference	
Parameters	Experimental	RTF model	Nonlinear model	Experimental vs. RTF model	Experimental vs. nonlinear model
30 °C	1.47 ± 0.3	1.80	1.50	22.5	2.0
30 °C+MC	1.52 ± 0.4	1.72	1.80	13.2	18.4
10 °C	2.02 ± 0.5	1.92	1.90	5.0	5.9

Appendage Kinematics: Simulations vs Experiments